PLOS ONE

Simulating an Infection Growth Model in Certain Healthy Metabolic Pathways of *Homo sapiens* for Highlighting Their Role in Type I *Diabetes mellitus* Using Fire-Spread Strategy, Feedbacks and Sensitivities

Somnath Tagore[1], Rajat K. De[2]*

1 Department of Biotechnology and Bioinformatics, Padmashree Dr. D. Y. Patil University, Navi Mumbai, India, **2** Machine Intelligence Unit, Indian Statistical Institute, Kolkata, India

Abstract

Disease Systems Biology is an area of life sciences, which is not very well understood to date. Analyzing infections and their spread in healthy metabolite networks can be one of the focussed areas in this regard. We have proposed a theory based on the classical forest fire model for analyzing the path of infection spread in healthy metabolic pathways. The theory suggests that when fire erupts in a forest, it spreads, and the surrounding trees also catch fire. Similarly, when we consider a metabolic network, the infection caused in the metabolites of the network spreads like a fire. We have constructed a simulation model which is used to study the infection caused in the metabolic networks from the start of infection, to spread and ultimately combating it. For implementation, we have used two approaches, first, based on quantitative strategies using ordinary differential equations and second, using graph-theory based properties. Furthermore, we are using certain probabilistic scores to complete this task and for interpreting the harm caused in the network, given by a 'critical value' to check whether the infection can be cured or not. We have tested our simulation model on metabolic pathways involved in Type I *Diabetes mellitus* in *Homo sapiens*. For validating our results biologically, we have used sensitivity analysis, both local and global, as well as for identifying the role of feedbacks in spreading infection in metabolic pathways. Moreover, information in literature has also been used to validate the results. The metabolic network datasets have been collected from the Kyoto Encyclopedia of Genes and Genomes (KEGG).

Competing Interests: The authors have declared that no competing interests exist.

* E-mail: rajat@isical.ac.in

Introduction

An important aspect of metabolic pathway analysis is studying the impact of infections or disease spread in healthy metabolic pathways. Tackling the growth of infection in a healthy metabolic pathway as well as curing it simultaneously is rather complex. Let us consider a scenario, wherein, a metabolite in a healthy metabolic network becomes infected due to some mutation or external perturbation. Moreover, a metabolite is said to be infected if its formation, in a metabolic pathway, is somehow impaired. The major problem lies in tracking the progress of this infection to other non-infected neighboring metabolites and understand the nature of this spread [1]. The result of such an infection may further give rise to in improper production of certain metabolites leading to improper functioning of the entire metabolic pathway. In case of a healthy metabolic network, tracking this path is very difficult. The reason is that prior probability of a healthy metabolite to be infected is difficult to predict. Moreover, once the metabolite is infected, it can infect its neighbors with an infection rate, and can also be cured with a

curing rate. Once cured or healthy, the metabolite is again prone to the infection. However, both infection and curing process may occur independently [2].

In this study we have implemented the forest fire strategy for analyzing the infection spread in a healthy metabolic pathway. The classical forest fire algorithm suggests that when fire erupts in a forest, it spreads to its surrounding trees, resulting in their further burning. At each step of this process, the burning trees have a probability of staying on fire and burning out, whereas the surrounding trees also have a probability of ignition [3]. This fundamental idea can be taken into consideration for studying the spread of infection in metabolic networks that are represented as directed graph format. Infection can be caused in the healthy metabolites via an infected metabolite, which can spread further and hence can be used to study the harm caused to the overall metabolic network [4]. In such cases, there is a possibility that either the metabolites are infected, safe or cured. Also, infections can be caused either by its nearest neighbors or its next-nearest neighbors. We have constructed a simulation model which can be used to study the infection caused in a network from infection

initiation, to spread and ultimately combating it. Moreover, we have used certain probabilistic scores to complete this task that results in interpreting the harm caused in a healthy metabolic network, given by certain 'critical value' for checking whether the infection can be cured or not [5]. Thus, any harm caused to any metabolite in the pathway can provide a clear picture of the overall infection spread. But, the difference between a metabolic pathway and forest is that in the former, there are no direct contact links, wherein contacts are linked as reaction links. Also, there are many other factors involved, such as, feedback links, presence of topological units, to name a few, which must be considered for predicting the cause and nature of the path of infection spread. We have used strategies such as feedback link prediction, sensitivity approaches for handling such instances (discussed in details later).

Recent literature shows that some basic disease models have been developed to analyze the spread of certain diseases in real-world networks. These models describe the susceptibility, infection scenario and recovery rates of populations from a particular disease. In all these models information related to infection progress is not taken into account because of the differences in response among individuals in a specific population. Moreover, based on the epidemiological studies of individuals, two standard models, namely, susceptible-infectious-recovered (SIR) and susceptible-infectious-susceptible (SIS), have been proposed (discussed in section 'Methodology') for analyzing the study of disease spread in populations [6]. These models work on determining the source of infection and then linking each infected individual to one another, as well as to a variable number of others to whom they transmitted the disease. It generated a network of individuals consisting of all the links through which infection spreads in course of a single disease outbreak. Furthermore, some contact-tracing approaches were also developed to identify all potential transmission contacts from a source individual. These approaches identified a new set of individuals who might have the tendency to get infected from some already infected individuals. It has been applied in cases of sexually transmitted diseases (STDs) where a contact is most easily defined. But, all these network-based studies are limited by fact that there is no simple way to relate the sensitivity of the results to the details of the network structure. We have studied the path of infection spread by developing an algorithm based on SIS model (discussed in section 'Methodology') [7].

To understand the feature of fire spread, we have selected two strategies, first, based on quantitative studies, and second, based on graphs. The first strategy implements the fire spread using mathematical models and expressions. We have used ordinary differential equations (ODEs) for this purpose. We use ODEs for representing the complete metabolic pathway, its constituents as well as their ongoing interactions. As these metabolic processes are dynamic in nature, modeling them using ODEs is extremely useful [8]. The second strategy, based on graph theory, considers connectivity patterns and other structure-based properties among metabolites for implementing the fire spread in the metabolic pathway. Here, we represent the metabolic pathways in the form of directed graphs. Since, we are proposing a computational strategy for understanding the fire spread process, it is essential to validate it biologically. The reason is that the strategy may work *in-silico* but may fail when implemented on a real dataset. For this purpose, we have modeled and analyzed a prevalent property of metabolic pathways, namely, occurrence of feedback reactions and

studied its role in disease spread [9]. Again, for this analysis, we have proposed a quantitative method. Furthermore, we have found that certain metabolites play a key role in disease spread and combat. For biological validation, we have used the technique of sensitivity analysis to understand the nature and property of these metabolites and their role in disease spread. Sensitivity analysis is a mathematical implementation of understanding the systematic change in the metabolic pathway due to perturbations, both internal and external (discussed in details in section 'Methodology') [10].

For testing our simulation tool, we have selected Type I *Diabetes mellitus* in *H. sapiens*. *Diabetes mellitus* is a metabolic disorder of multiple aetiology that is characterized by chronic hyperglycaemia affecting carbohydrate, fat and protein metabolism, which results from improper insulin production. *Diabetes mellitus* affects in various manners, which include long-term damage, dysfunction and failure of multiple organs. Furthermore, certain genes play a vital role in the development of *Diabetes mellitus*. To date, more than 250 candidate genes have been investigated, and results have shown a very high variability in gene association with *Diabetes mellitus* [11]. But, it is yet to be identified all the gene mutations that put a person at risk for *Diabetes mellitus*. Even if mutations are known, some investigations have found that people with low risk genes can still develop *Diabetes mellitus*. Moreover, it has been observed that the combination of susceptible genes and environmental factors may initiate this disease process that is associated with the formation of an autoimmune response to the insulin-producing cells. This autoimmune reaction is reflected by the presence of antibodies against prominent antigens in the pancreatic β-cells [12].

Type I is usually characterized by the presence of anti-Glutaric acid decarboxylase (GAD), islet cell or insulin antibodies which identify the autoimmune processes that lead to β-cell destruction. The insulin gene (INS) is the second well established susceptible locus in *Diabetes mellitus*. It contributes about 10% toward *Diabetes mellitus* susceptibility [13]. We have analyzed the onset of Type I *Diabetes mellitus* in *H. sapiens* by studying the role of GAD and INS genes in metabolic pathways involving Type I *Diabetes mellitus* from a Systems Biology perspective. For this purpose, we have used the SBML format of metabolic pathway datasets under Type I *Diabetes mellitus* of *H. sapiens* for our study. We have downloaded the metabolic pathway datasets which have shown role in the expression of GAD and INS genes, known from Kyoto Encyclopedia of Genes and Genomes (KEGG) [14], and used KEGG2SBML tool for converting them in SBML format [15].

Materials and Methods

Here we describe the method we have developed for implementing fire spread in healthy metabolic networks in *H. sapiens*, analyzing their tendency to become infected giving rise to Type I *Diabetes mellitus*. We have collected the metabolic pathway datasets involving GAD and INS genes from Kyoto Encyclopedia of Genes and Genomes (KEGG). One of the criteria for handling our algorithm requires input to be given in Systems Biology Markup Language (SBML) format. We used the KEGG2SBML tool for converting the metabolic pathway datasets from KEGG to SBML format [15]. Systems Biology Markup Language (SBML) is an XML-based language for representing biological network-based models. Any biochemical reaction in a metabolic pathway can be represented into a number of XML-based elements like reactant species, product species, reactions, stoichiometric rates,
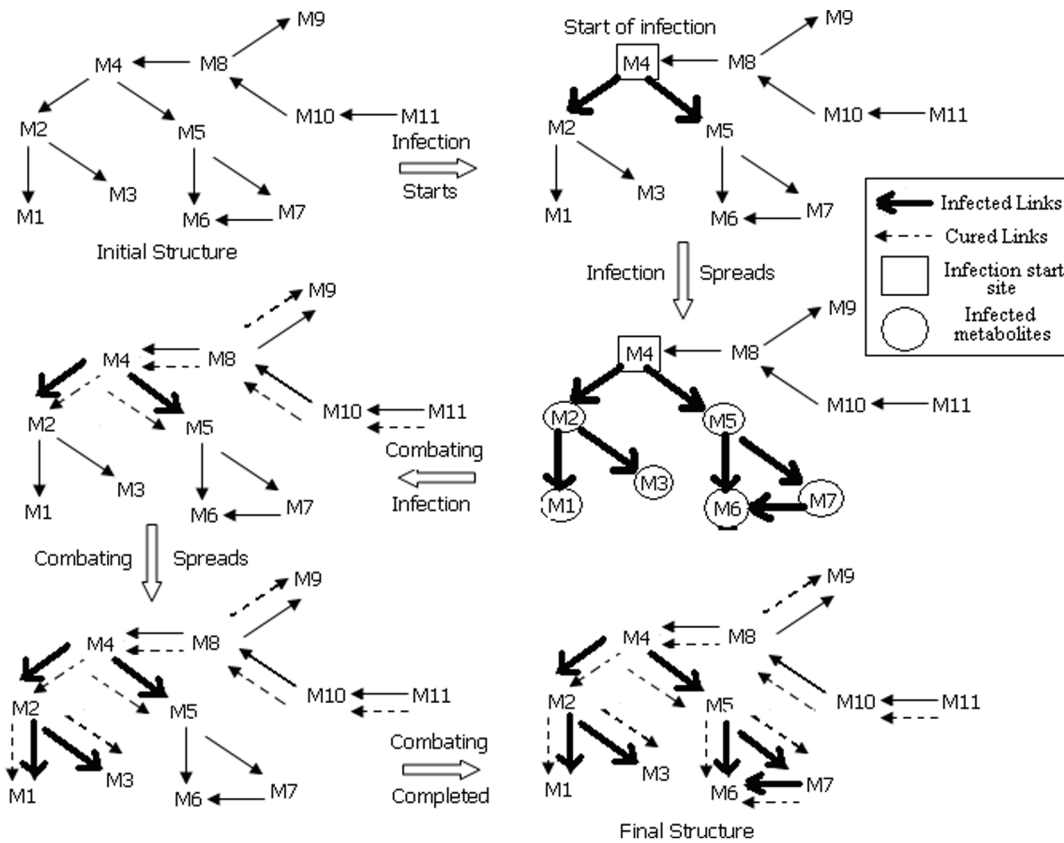
Figure 1. Analyzing the spread of infection and combat process in a hypothetical metabolic network; nodes represent metabolites, edges represent reaction links, bold lines signify infection, dotted lines signify combat.
doi:10.1371/journal.pone.0069724.g001

and some other parameters necessary for the reactions to occur [16]. Similarly, a network of reactions can also be represented in the same manner. An SBML representation consists of certain standard modules, like *compartment* which acts as a container of finite volume where reactions take place, *species* which represents an entity that takes part in a reaction, *reaction* which describes some transformation process converting one or more species, *parameter* which describes a quantity taking part in a reaction process, *unit definition* which specifies a name of a unit used in the expression of quantities in a reaction model, and *rule* which acts as a mathematical expression that is added to the model equations constructed from the set of reactions.

The complete methodology is divided into *five* steps, which are performed one after another in successive manner. The *first* step is quantitative formulation of the metabolic pathways using ordinary differential equations (ODE), which deals with conversion of the entire metabolic pathways in the form of ODEs. This is one of the preliminary aspects of quantitative modeling. The *second* step is fire spread analysis, which involves modeling the fire spread mathematically using information from the *first* step and implementing it into the healthy metabolic pathway. The *third* step is handling the presence of feedback reactions, analyzing their role in fire spread and combat. This step has two sub-steps, namely, modeling feedback reactions and identifying them in the metabolic

pathways. The *fourth* step deals with analyzing the sensitivity threshold of metabolic pathways against this fire spread. We performed both local as well as global sensitivity analysis. The *fifth* and last step is damage analysis, which calculates the extent of infections that spread throughout the metabolic pathway and the metabolites that remain uneffected/healthy or which have become cured after becoming susceptible to infection attack. For implementation purpose, we selected glutamate metabolism for further explanation.

Quantitative formulation of metabolic pathways using ordinary differential equations (ODEs)

Here, we have used ODEs to model the entire glutamate metabolism in terms of the metabolites participating in various reactions as shown below. Our intention of performing this step was to model the spread of infection mathematically, for which initial structure of the healthy glutamate metabolism needs to be converted into ODE form. For this purpose, we assumed some notations, namely, *a* to *i*, which represent genes, and V_{def}, default volume of the compartment. The unit-wise representation of the metabolites is *mol/l*. The other parameters involved are the kinetic parameters whose initial values are assumed to be 1 [17]. The ODEs of glutamate metabolism in terms of its participating non-pool metabolites are as given below.

$$\frac{d}{dt}([L-glutamate].V_{def}) =$$

$$+ V_{def} \cdot \left([g] \cdot \frac{1.[5-phosphoribosylamine].V_{def}.[L-glutamate].V_{def}}{1 + [5-phosphoribosylamine].V_{def}.[L-glutamate].V_{def} - [5-phospho-\alpha-D-ribose-1-diphosphate].V_{def}} \right)$$

$$+ V_{def} \cdot \left([h] \cdot \frac{1.[L-glutamate].V_{def}}{1 + [L-glutamate].V_{def}} \right) - V_{def} \cdot \left(\frac{1.[b].[L-glutamine].V_{def}}{1.1 + [L-glutamine].V_{def}.[D-fructose-6-phosphate].V_{def} - [L-glutamate].V_{def}.[D-glucosamine-6-phosphate].V_{def}} \right)$$

$$- V_{def} \cdot \left(\frac{1.[c].[L-glutamine].V_{def}}{1.1 + [L-glutamine].V_{def} - [L-glutamate].V_{def}} \right) \frac{d}{dt}([L-glutamine].V_{def}) =$$

$$+ V_{def} \cdot \left([b] \cdot \frac{1.[L-glutamine].V_{def}.[D-fructose-6-phosphate].V_{def}}{1 + [L-glutamine].V_{def}.[D-fructose-6-phosphate].V_{def} - [D-glucosamine-6-phosphate].V_{def}} \right)$$

$$+ V_{def} \cdot \left([c] \cdot \frac{1.[L-glutamine].V_{def}}{1 + [L-glutamine].V_{def}} \right) + V_{def} \cdot \left([d] \cdot \frac{1.[L-glutamate-5-semialdehyde].V_{def}}{1 + [L-glutamate-5-semialdehyde].V_{def}} \right)$$

$$- V_{def} \cdot \left(\frac{1.[z].[L-glutamate].V_{def}}{1.1 + [L-glutamate].V_{def} - [4-aminobutanoate].V_{def}} \right)$$

$$- V_{def} \cdot \left(\frac{1.[a].[L-glutamate].V_{def}}{1.1 + [L-glutamate].V_{def} - [2-oxoglutarate].V_{def}} \right)$$

$$\frac{d}{dt}([4-aminobutanoate].V_{def}) = + V_{def} \cdot \left([z] \cdot \frac{1.[L-glutamate].V_{def}}{1 + [L-glutamate].V_{def}} \right)$$

$$- V_{def} \cdot \left(\frac{1.[x].[4-aminobutanoate].V_{def}.[2-oxoglutarate].V_{def}}{1.1 + [4-aminobutanoate].V_{def}.[2-oxoglutarate].V_{def} - [succinatesemialdehyde].V_{def}.[L-glutamate].V_{def}} \right)$$

$$\frac{d}{dt}([5-phosphoribosylamine].V_{def})$$

$$= - V_{def} \cdot \left(\frac{1.[g].[5-phosphoribosylamine].V_{def}.[L-glutamate].V_{def}}{1.1 + [5-phosphoribosylamine].V_{def}.[L-glutamate].V_{def} - [L-glutamine].V_{def}.[5-phospho-\alpha-D-ribose-1-diphosphate].V_{def}} \right)$$

$$\frac{d}{dt}([D-glucosamine-6-phosphate].V_{def}) = + V_{def} \cdot \left([b] \cdot \frac{1.[L-glutamine].V_{def}.[D-fructose-6-phospate].V_{def}}{1 + [L-glutamine].V_{def}.V_{def}.[D-fructose-6-phospate].V_{def} - [L-glutamate].V_{def}} \right)$$

$$\frac{d}{dt}([succinatesemialdehyde].V_{def}) =$$

$$+ V_{def} \cdot \left([x] \cdot \frac{1.[4-aminobutanoate].V_{def}.[2-oxoglutarate].V_{def}}{1 + [4-aminobutanoate].V_{def}.[2-oxoglutarate].V_{def} - [L-glutamate].V_{def}} \right)$$

$$- V_{def} \cdot \left(\frac{1.[y].[succinatesemialdehyde].V_{def}}{1.1 + [succinatesemialdehyde].V_{def}.[succinate].V_{def}} \right)$$

$$\frac{d}{dt}([succinate].V_{def}) = + V_{def} \cdot \left([y] \cdot \frac{1.[succinatesemialdehyde].V_{def}}{1 + [succinatesemialdehyde].V_{def}} \right)$$

$$\frac{d}{dt}([2-oxoglutarate].V_{def}) = + V_{def} \cdot \left([a] \cdot \frac{1.[L-glutamate].V_{def}}{1 + [L-glutamate].V_{def}} \right)$$

$$+ V_{def} \cdot \left([f] \cdot \frac{1.[2-oxoglutarate].V_{def}}{1 + [2-oxoglutarate].V_{def}} \right)$$

$$- V_{def} \cdot \left(\frac{1.[x].[2-oxoglutarate].V_{def}.[4-aminobutanoate].V_{def}}{1.1 + [2-oxoglutarate].V_{def}.[4-aminobutanoate].V_{def} - [succinatesemialdehyde].V_{def}.[L-glutamate].V_{def}} \right)$$

$$\frac{d}{dt}([2-oxoglutaramate].V_{def})$$

$$= - V_{def} \cdot \left(\frac{1.[f].[2-oxoglutaramate].V_{def}}{1.1 + [2-oxoglutaramate].V_{def} - [2-oxoglutarate].V_{def}} \right)$$

$$\frac{d}{dt}([D-fructose-6-phosphate].V_{def}) =$$

$$- V_{def} \cdot \left(\frac{1.[b].[D-fructose-6-phosphate].V_{def}}{1.1 + [D-fructose-6-phosphate].V_{def}.[L-glutamate].V_{def} - [D-glucosamine-6-phosphate].V_{def}} \right)$$

$$\frac{d}{dt}([5-phsopho-\alpha-D-ribose-1-diphosphate].V_{def})$$

$$= + V_{def} \cdot \left([g] \cdot \frac{1.[5-phosphoribosylamine].V_{def}.[L-glutamate].V_{def}}{1 + [5-phosphoribosylamine].V_{def}.[L-glutamate].V_{def} - [L-glutamine].V_{def}} \right)$$

$$\frac{d}{dt}([L-glutamate-5-semialdehyde].V_{def}) =$$

$$- V_{def} \cdot \left(\frac{1.[d].[L-glutamate-5-semialdehyde].V_{def}}{1.1 + [L-glutamate-5-semialdehyde].V_{def} - [L-glutamine].V_{def}} \right)$$

$$\frac{d}{dt}([L-aspartate].V_{def}) = - V_{def} \cdot \left(\frac{1.[i].[L-aspartate].V_{def}}{1.1 + [L-aspartate].V_{def} - [N-carbamoyl-L-aspartate].V_{def}} \right)$$

$$\frac{d}{dt}([N-carbamoyl-L-aspartate].V_{def}) = + V_{def} \cdot \left([i] \cdot \frac{1.[L-aspartate].V_{def}}{1 + [L-aspartate].V_{def}} \right)$$

Now, considering the ODE for $L-aspartate$, we observe that it participates in reaction 12 only, where it acts as a reactant species. Thus, $1.[i].[L-aspartate].V_{def}$ in ODE stands for reactant contribution whereas $1.1+[L-aspartate].V_{def}-[N-carbamoyl-L-aspartate].V_{def}$ stands for product as well as contribution of $L-aspartate$ associated with *carbamoylphosphate* as reactants [18]. Similarly, the ODE representations of other metabolites have also been constructed in identical manner. Thus, modeling metabolic pathways quantitatively helped us to understand the initial structure of healthy metabolic pathways before being subjected to disease spread. Also, now we are in a position to understand the spread of disease in this healthy metabolic pathway and represent it mathematically for further simulation studies.

Fire spread analysis

One of the widely analyzed epidemic models is the susceptible-infected-removed or SIR models [16]. In this work, we implemented the SIR model with certain modifications in four healthy metabolic pathways of *H. sapiens* to analyze their susceptibility for T1D. The original SIR model was first proposed by Lowell Reed and Wade Hampton Frost in 1920. It discussed the growth of an epidemic in a population of individuals, where the population is divided into three states, namely, susceptible (S), infection (I) and removed (R). Susceptible individuals are those who have higher chance of getting infected from some already infected individuals, whereas removed state corresponds to those individuals who are either dead or removed from the populations [19]. We have discussed this section under two sub-headings, namely, mathematical modeling of fire and implementation of fire spread. In mathematical modeling of fire, we discuss the various notations regarding the SIR model in the form of ODEs, which we generate from the already generated schema of ODEs of healthy metabolic pathways. The second subSection S4eals with the actual implementation of the fire spread in glutamate metabolism of *H. sapiens* for checking its susceptibility against infection spread. Fig. 1

represents the architecture of the path of infection spread in a hypothetical pathway.

Mathematical modeling of fire. In the previous section, we generated the ODEs for the healthy metabolites in glutamate metabolism which are still uneffected from infection spread. Now, we focus on the structure of the same metabolic pathway after it gets infected. For the same purpose, certain notations have been considered, namely, $M =$ network size, $N =$ total number of metabolites getting inserted randomly into M, $P =$ total number of metabolites that are susceptible to infection spread, $I_{act} =$ total number of metabolites that are actively infected, $I_{pas} =$ total number of metabolites that are passively infected, $N_P =$ probability that a susceptible metabolite is not cured, $C_{act} =$ curing rate (active), $C_{pas} =$ curing rate (passive), $I =$ total number of infected metabolites, $q =$ number of infected metabolites getting degenerated, $\beta =$ breakdown rate, $\alpha =$ infection rate, $\mu =$ susceptibility rate, $\epsilon =$ degeneracy rate, and $I' =$ number of cured metabolites.

First, we model the rate of change of the structure of pathway with time against possible infection attack. Thus, we have

Change in number of metabolites that are susceptible to infection attack

$=$ Current pathway architecture $-$ metabolites that are infected directly or actively with a certain infection rate $-$ susceptible metabolites getting infected with a certain susceptibility rate $+$ metabolites that are cured actively with active curing rate $+$ metabolites that are cured passively with passive curing rate [20]

$i.e., \dfrac{dP}{dt} = \sum(M,N) - \alpha.I_{act}.P - \mu.P + C_{act}.I_{act} + C_{pas}.I_{pas}$ Next, we find change in number of passive infected metabolites with time, i.e.,

Change in number of infected metabolites in passive manner

$=$ Number of susceptible metabolites that are actively infected $-$ breakdown of already actively infected metabolites $-$ curing of infected metabolites with passive curing rate $-$ susceptibility of
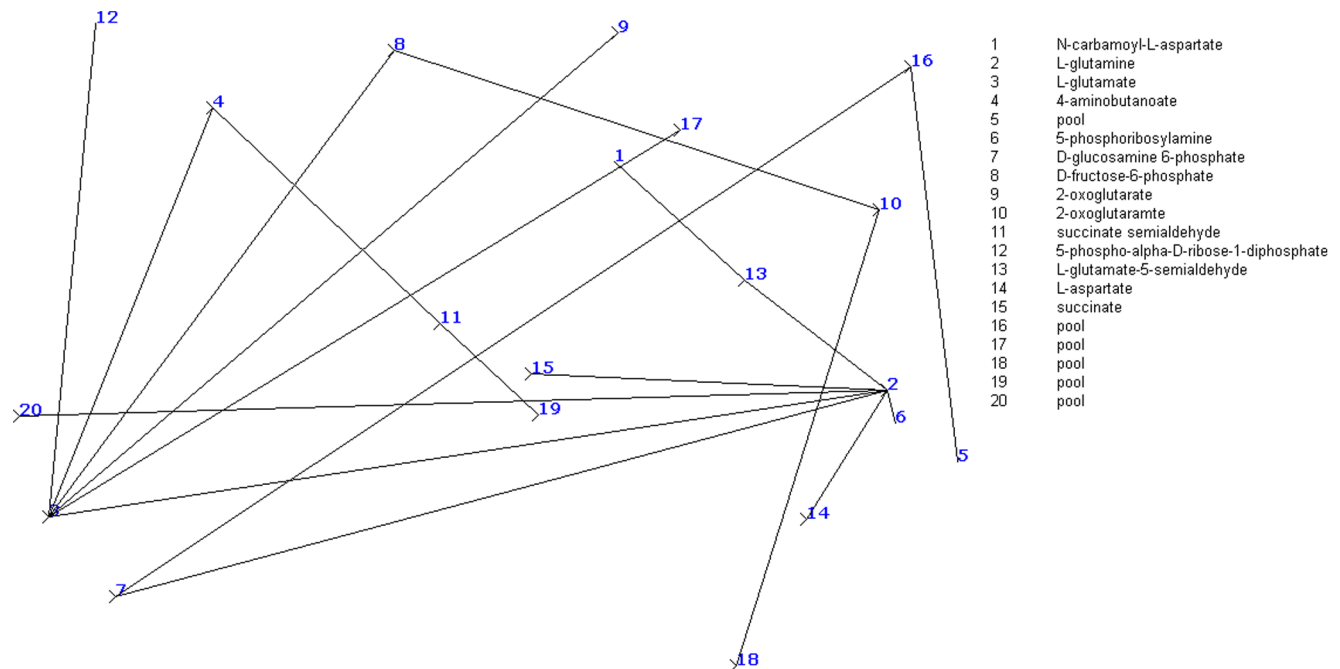
Figure 2. Directed graph-based representation of *glutamate* metabolism, as generated by our simulation model; nodes represent metabolites and edges represent reaction links.
doi:10.1371/journal.pone.0069724.g002

The figure legend list reads:

1 N-carbamoyl-L-aspartate
2 L-glutamine
3 L-glutamate
4 4-aminobutanoate
5 pool
6 5-phosphoribosylamine
7 D-glucosamine 6-phosphate
8 D-fructose-6-phosphate
9 2-oxoglutarate
10 2-oxoglutaramte
11 succinate semialdehyde
12 5-phospho-alpha-D-ribose-1-diphosphate
13 L-glutamate-5-semialdehyde
14 L-aspartate
15 succinate
16 pool
17 pool
18 pool
19 pool
20 pool

cured metabolites getting infected again [20] $i.e., \frac{dI_{pas}}{dt} = (I-q).\alpha.I_{act}.P - \beta_{act}.I_{pas} - C_{pas}.I_{pas} - \mu.I_{pas}$ Similarly, for identifying the change in number of actively infected metabolites with time, we have,

Change in number of infected metabolites in active manner

= Number of metabolites getting degenerated due to infection of metabolites (both susceptible and healthy) in active manner+ breakdown of infected metabolites−curing of infected metabolites with a certain curing rate−susceptibility of already infected metabolites to be getting infected again−degeneration of the infected metabolites with a degeneracy rate [20] $\frac{dI_{act}}{dt} = q.\alpha.I_{act}.P + \beta_{act}.I_{pas} - C_{act}.I_{act} - \mu.I_{act} - \epsilon.I_{act}$ Furthermore, in case of healthy metabolic pathways, (i.e., in absence of any infection), $\frac{dP}{dt}=0, \frac{dI_{act}}{dt}=0, \frac{dI_{pas}}{dt}=0$ i.e.,

$\sum(M,N) - \alpha.I_{act}.P - \mu.P + C_{act}.I_{act} + C_{pas}.I_{pas} = 0$

$(I-q).\alpha.I_{act}.P - \beta_{act}.I_{pas} - C_{pas}.I_{pas} - \mu.I_{pas} = 0$

$q.\alpha.I_{act}.P + \beta_{act}.I_{pas} - C_{act}.I_{act} - \mu.I_{act} - \epsilon.I_{act}$

Also, in initial state, $I_{act}=0$, $I_{pas}=0$, and $M+N-\mu.P=0$. Furthermore, we have also considered the various transition events associated with the healthy metabolic pathways, after getting infected [20]. They are, $P \rightarrow P+1, I \rightarrow 1, P \rightarrow R (recovered)$; $r_1(rate) = \rho_1.M$ (increase in M) $P \rightarrow P-1, I \rightarrow 1, P \rightarrow R$; $r_2(rate) = \rho_2.P$ (decrease in M)

$$P \rightarrow P, I \rightarrow I-1, P \rightarrow R; r_3(rate) = \rho_2.I \qquad \text{(decrease)}$$

$$P \rightarrow P-1, I \rightarrow I+1, R \rightarrow R; r_4(rate) = \frac{\rho_3.I.P}{M} \qquad \text{(infection)}$$

$$P \rightarrow P, I \rightarrow I-1, R \rightarrow R+1; r_5(rate) = \rho_4.I \qquad \text{(recovery)}$$

$$P \rightarrow P, I \rightarrow I+1, R \rightarrow R; r_6(rate) = \rho_3 \qquad \text{(infection)}$$

ρ_1, ρ_2 = force of infection, ρ_3 = coefficient of transmission, $\rho_4 = M - I'$ = critical factor

One of the most important factors associated with this nomenclature is the critical factor (ρ_4), which represents the actual number of metabolites that remain uneffected after disease spread. As ρ_4 increases, the resistivity and robustness of the metabolic pathway also increases and vice-versa. The next subSection S4eals with the actual implementation of our model in glutamate metabolism of *H. sapiens*.

Implementation of fire spread. For visual purpose, we represented the metabolic pathways as directed graphs, where metabolites are represented as nodes and enzymes are represented
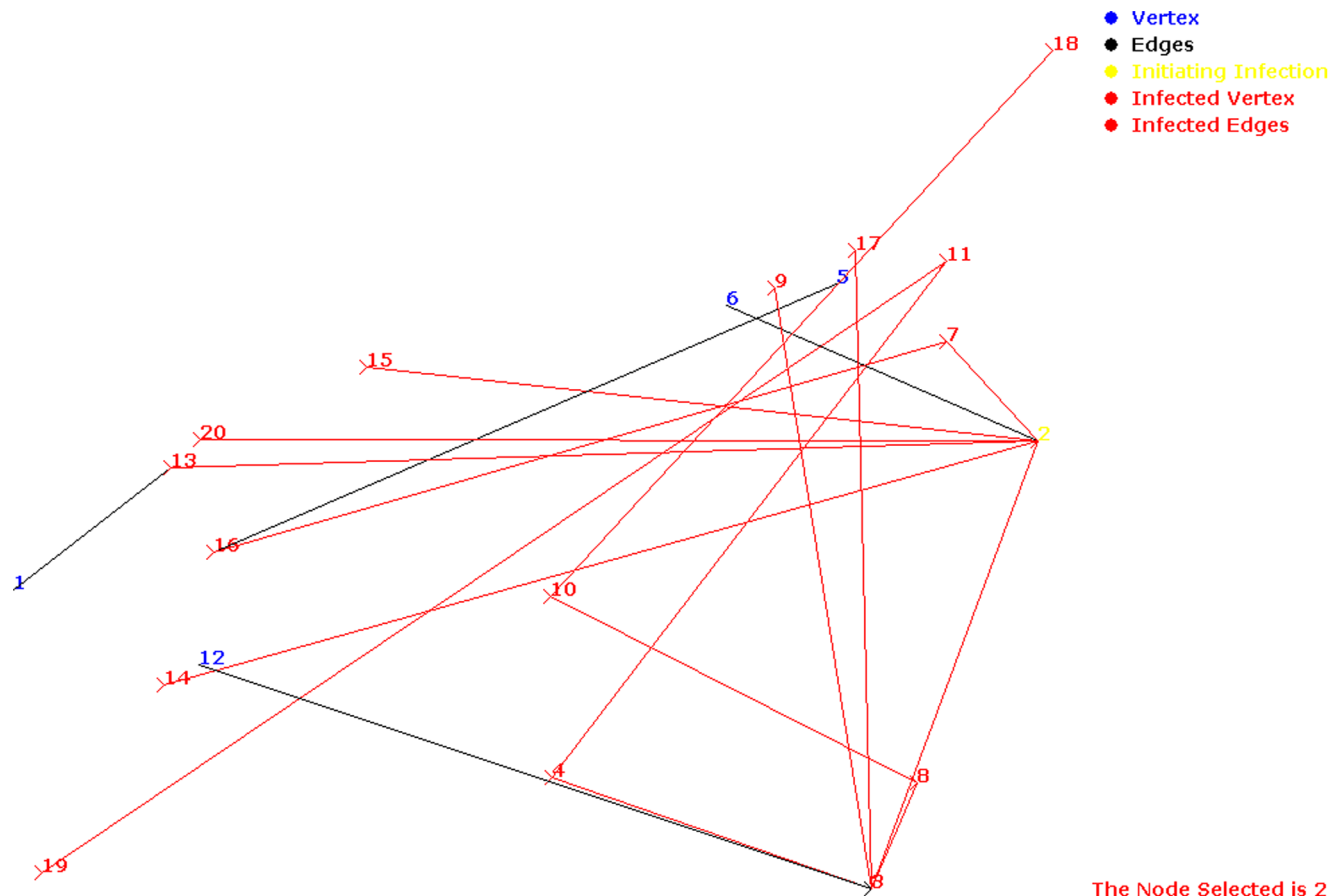
Figure 3. Spread of infection in glutamate metabolism in *H. sapiens* having infection start site as '2'.
doi:10.1371/journal.pone.0069724.g003
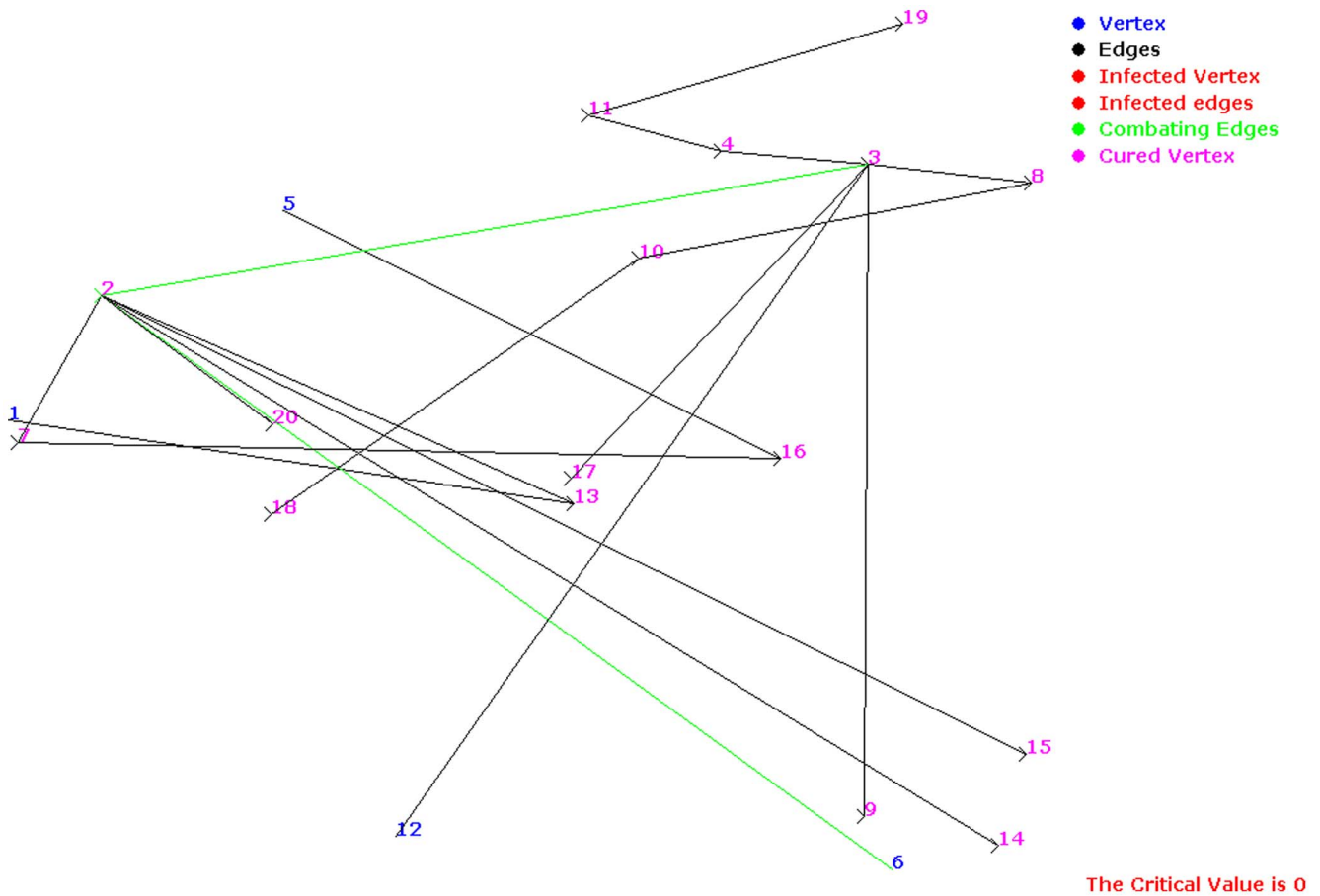
Figure 4. Combat process in glutamate metabolism in *H. sapiens* having infection start site as '3'.
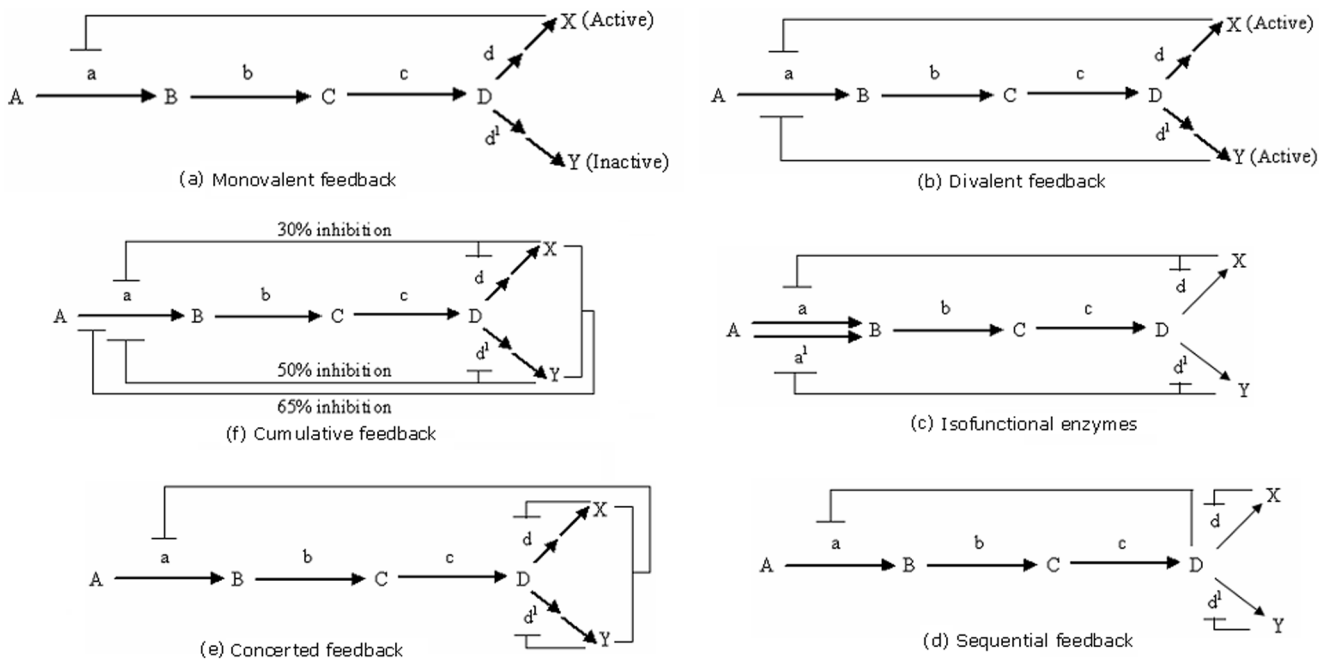
Figure 5. Schematic representation of certain feedback reactions that are predominant in metabolic pathways in *H. sapiens*; A–D, X and Y denote metabolites, and a–d and d' signify reaction links/genes.

as edges [21]. Fig. 2 illustrates the glutamate metabolism in *H. sapiens* in directed graph format as generated by our algorithm.

As discussed in the previous subsection, an infected metabolite can recover back, but may again become susceptible to infection [4]. In a standard SIR model it is assumed that those which are getting immunized do not get infected again, whereas in case of our model we do not consider any metabolite to become immunized to the infection spread and consider them equally susceptible to other infected metabolites against infection [22]. In a metabolic pathway, we consider that the infection spread happens through the interconnected links among the metabolites [23]. We also consider that the most important aspect in this case is designing effective strategies for preventing and restricting the outbreak of infection. One of the effective approaches in this case is curing the infected metabolites and vaccinating the uneffected ones with a probability proportional to their connectivities, so that a greater proportion of metabolites of high connectivity are vaccinated than metabolites with low connectivity. Another strategy is specifically targeting the hub (highly connected) metabolites by vaccinating all metabolites of connectivity higher than some threshold value [6].

The graph-theory based implementation initiates with representing the input metabolic pathway (in SBML format) into a directed graph $G(V,E,\omega)$, where V is a set of metabolites, E is a set of reaction links and ω is a set of mapping functions that maps every link onto some ordered pair of metabolites (v_i, v_i^l). We also consider two structural attributes, namely, 'front propagation $d^+(v_i)$' and 'back propagation $d^-(v_i)$', i.e., number of outgoing and incoming links to a metabolite. For initializing the event of fire or infection, an initial metabolite, v_i is selected that acts as the start or ignition site [7]. Thus, we consider that infection spreads from this start site to other neighboring metabolites through their connecting links. Considering glutamate metabolism, the initial pathway structure before infection spread is, $M=14, N=0, P=0, I_{act}=0, I_{pas}=0, N_p=0, C_{act}=0, C_{pas}=0, I=0, q=0, \beta=0, \alpha=0, \mu=0, \epsilon=0, I'=0$. Now, fire spreads from v_i, through the links connecting it to its neighboring metabolites, based upon two factors, namely, 'Burning Probability (BP)' and 'Combating Probability (CP)'. The neighboring metabolites for a particular v_i is found out from ω. 'BP' is defined as the chance of a metabolite to become infected due to a neighboring infected metabolite where $BP(v_i) = \dfrac{1}{d^+(v_i)}$. Similarly, 'CP' is defined as the chance of an infected node to become cured, where $CP(v_i) = \dfrac{1}{d^-(v_i)}$ [23].

Here, we define a metabolite as 'infected' when it loses its functionality, due to some mutation and external perturbation, and becomes inefficient to form a useful product. Also, a metabolite is termed to be infected if its formation, in a metabolic pathway, is somehow impaired. We assume that higher the connectivity of this metabolite, more the probability that its

neighboring metabolites are infected. Also, if the metabolite is completely infected, it no longer participates in any other reaction, thus $d^+(v_i)$ becomes 0. This state is achieved when curing fails. A 'cured' metabolite is that which has large number of alternate and parallel paths of its production. The reason for considering an infected metabolite to be cured is that even if it becomes infected by a path leading to its destruction, it can be produced by an alternate path. It can be found by keeping a track on the incoming links, i.e., $d^-(v_i)$. For example, in Fig. 3, $BP(v_4)=0.5$, $BP(v_3)=1.0$, $BP(v_2)=0.5$, whereas $CP(v_4)=1.0$, $CP(v_6)=0.5$, to name a few.

Infection spreads from initial metabolite till the path ends where the value of $d^+(v_i)$ is 0 and 'BP' is minimum, i.e., when no further link is present connecting the infected metabolite to other healthy metabolites. All the infected metabolites are included in the set v_{in}. Once the infection has totally spread in the pathway, the factor taken into consideration is 'CP'. We also store the metabolites connected to an infected metabolite in the set v_{in}^l. After a metabolite v_i is infected, combating the infection will take place when the level of 'CP' is high [24]. Here, at each step the probability of combat for each metabolite changes according to the spread of infection and their bypasses. For example, $BP(v_4)=0.5$, $CP(v_4)=1.0$. Thus, the probability that v_4 will be cured is always high. The same was the case with v_2, where $BP(v_2)=0.5$ and $CP(v_2)=1.0$. Thus, chances of v_4 and v_2 to be cured were quite high. The above simulation was with respect to the structural parameters associated with the pathway. But, biologically, only structural parameters could not be taken into consideration for simulation purpose. Thus, for adhering the biological aspect of our model, we calculated the ODE values too. Thus taking $v_i=2$, various factors associated with it were $M=14, N=0, P=6$ (metabolites that were not directly linked to v_i but are susceptible), $I_{act}=7, I_{pas}=6, N_p=0, C_{act}=0.14, C_{pas}=0.16, I=14, q=0, \beta=0, \alpha=1, \mu=0.42, \epsilon=0, I'=0$. Thus, $\dfrac{dP}{dt}=-28.58, \dfrac{dI_{pas}}{dt}=584.52, \dfrac{dI_{act}}{dt}=-3.92, \rho_4=0$. Thus, critical factor was 0, i.e., size of the pathway did not change and all infected metabolites were cured (Figs. 3, 4).

Analyzing feedbacks

As we deal with metabolic pathways, there are various ongoing processes that we need to consider so that our simulation is successful and biologically relevant. One of the most important properties in metabolic pathways is the presence of feedback reactions, which can drastically effect their overall functionality. So, we studied the existence of feedbacks and related them to our model. This subsection explains the basic implementation strategy followed by us for identification of feedbacks [9]. The different categories of feedback reactions occurring in metabolic pathways are shown in Fig. 5, 6.

Modeling feedback reactions. We considered a model $X_a \rightarrow X_b$ for a metabolic reaction having one substrate and one
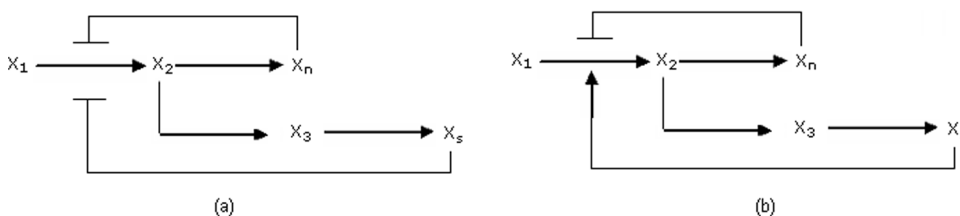
Figure 6. Schematic representation of a feedback loop, as found in metabolic pathways in *H. sapiens*, X_1, X_2, X_3, X_4, X_5 and X_n denote metabolites.
doi:10.1371/journal.pone.0069724.g006

product formation. Also, the reaction is inhibited by other metabolites present in the pathway. Furthermore, we denote the reaction rate for such a reaction by $\gamma_{ab}(x_a, x^{[m]})$, where x_a is concentration of metabolites X_a in cell and $x^{[m]}$ is the vector containing concentration of other metabolites inhibiting the reaction $X_a \rightarrow X_b$. It may be noted that γ_{ab} can also represent a sum of several parallel reactions that may be catalyzed by several isofunctional enzymes [25]. Moreover, larger the concentration of inhibitor, the reaction becomes much slower. Thus, we have, $\forall a, b$ such that, $X_a \rightarrow X_b$, the function $\gamma_{ab}(x_a, x^{[m]})$ is locally Lipschitz on $\mathbb{R}_+ \times \mathbb{R}_+^{n_m}$, satisfying $\gamma_{ab}(0, x^{[m]}) = 0$, increasing in x_a for $x_a \geq 0$ and decreasing in $x_i^{[m]}$ for $x_i^{[m]} \geq 0$. Quantitatively, we also study the presence of feedbacks using ODEs and graphs, especially, the arborescent property of graphs [25].

A directed graph is known an arborescence if, from a given node x (root node), there is exactly one elementary path to some other node y. Thus, in a metabolic pathway the species involved are $x_1, x_2, ..., x_n$ and the inhibiting reactions descend from the root $x_1 \rightarrow x_m$, inhibited by metabolites from the sub-arborescence rooted in x_m, we define the mass-balance dynamical model in the form, $\frac{dx}{dt} = \psi(x) - \phi.x + p.Q$, where ψ includes all reaction rates, $\phi \geq 0$ represents growth rate of the cell, $Q = (1,0,...,0)^T$, $p =$ scalar quantity, denotes constant supply rate of x_1 at root, $x = (x_1,...,x_n)^T \epsilon \mathbb{R}_+^n$, x_i is the molar fraction of metabolite x_1 inside cell [25]. Thus, using arborescence theory, we represent the root metabolite as $x_1 : \frac{dx_1}{dt} = c - \sum_{k \in \rho(1)} \gamma_{1k}(x_1, x^{[k]}) - \phi.x_1$ Here, $\rho(j) = \{k | x_1 \rightarrow x_k\}$ belong to the pathway. It defines the set of all metabolites that were produced by reactions having x_i as substrate, c as a constant factor. Similarly, there were intermediate metabolites, $x_j = (x_i \rightarrow x_j) : \frac{dx_j}{dt} = \gamma_{ij}(x_i, x^{[j]}) - \sum_{k \in \rho(j)} \gamma_{jk}(x_j) - \phi.x_j$ Lastly, for boundary metabolites, $x_j : \frac{dx_j}{dt} = \gamma_{ij}(x_i, x^{[j]}) - \gamma_{j0}(x_j) - \phi.x_j$

For understanding the stability of the network, $X_1 \rightarrow X_2 \rightarrow ... \rightarrow X_n$, we assumed that there was only one sequential feedback inhibition [25]. Thus, the velocity of each enzymatic reaction $X_i \rightarrow X_{i+1}$ is represented by the Michaelis-Menten kinetic function, $\gamma_i(x_i) = \frac{a_j x_i}{k_i + x_i}$ Here, x_i is intracellular molar fraction of X_i, a_i is maximal velocity and k_i is half-saturation constant. Also the velocity of $X_1 \rightarrow X_2$ is inhibited by the last metabolite with an inhibition function, $\gamma_\alpha(x_n) = \frac{1}{1 + \alpha.x_n}$ Thus, we have,

$$\frac{dx_1}{dt} = -\frac{a_1 x_1}{(k_1 + x_1)(1 + \alpha.x_n)} - \phi.x_1 - c$$
$$\frac{dx_2}{dt} = -\frac{a_1 x_1}{(k_1 + x_1)(1 + \alpha.x_n)} - \frac{a_2 x_2}{(k_2 + x_2)} - \phi.x_2$$
$$\frac{dx_i}{dt} = -\frac{a_{i-1} x_{i-1}}{(k_{i-1} + x_{i-1})} - \frac{a_i x_i}{(k_i + x_i)} - \phi.x_i, 3 \leq i \leq n$$

Here, $n \geq 3$, $x = (x_1,...,x_n)^T \epsilon \mathbb{R}^n$, $a_i, k_i s, c, \phi, \alpha$ are positive constants. Now, if both x_n and x_s inhibits (Fig. 6) $x_1 \rightarrow x_2$,

$$\frac{dx_1}{dt} = -\frac{a_1 x_1}{(k_1 + x_1)(1 + \alpha.x_n)(1 + \beta.x_s)} - \phi.x_1 - c$$
$$\frac{dx_2}{dt} = -\frac{a_1 x_1}{(k_1 + x_1)(1 + \alpha.x_n)} - \frac{a_2 x_2}{(k_2 + x_2)} - \phi.x_2$$
$$\frac{dx_3}{dt} = -\frac{a_2 x_2}{(k_2 + x_2)(1 + \beta.x_s)} - \frac{a_3 x_3}{(k_3 + x_3)} - \phi.x_3$$
$$\frac{dx_i}{dt} = -\frac{a_{i-1} x_{i-1}}{(k_{i-1} + x_{i-1})} - \frac{a_i x_i}{(k_i + x_i)} - \phi.x_i$$

Finally, if x_n inhibits $x_1 \rightarrow x_2$ (65%) and x_s activates $x_1 \rightarrow x_2$ (35%),

$$\frac{dx_1}{dt} = -\frac{(a_1 x_1)(1 + \beta.x_s)}{(k_1 + x_1)(1 + \alpha.x_n)} - \phi.x_1 - c$$
$$\frac{dx_2}{dt} = -\frac{a_1 x_1}{(k_1 + x_1)(1 + \alpha.x_n)} - \frac{a_2 x_2}{(k_2 + x_2)} - \phi.x_2$$
$$\frac{dx_3}{dt} = -\frac{(a_2 x_2)(1 + \beta.x_s)}{(k_2 + x_2)} - \frac{a_3 x_3}{(k_3 + x_3)} - \phi.x_3$$

With all these notations regarding feedbacks that we generated, the ultimate problem was to define certain algorithms to identify and characterize them, so that they could be further analyzed. The next subsection highlights some algorithms that we devised to identify feedbacks in metabolic pathways.

Identifying feedback reactions. All the algorithms for identifying and analyzing feedback reactions were based on identifying a pattern based on graph-based properties in metabolic pathways. The property of graphs that we used were isomorphism and arborescence. The algorithm proposed by us were for identifying feedback patterns, feedback activation, feedback inhibition, monovalent link prediction, divalent link prediction, iso-functional enzyme link prediction, sequential link prediction, concerted links prediction, and cumulative links respectively.

Symbols used

1. $m =$ pattern
2. $G =$ pathway graph
3. $g =$ subgraph in G
4. $c_m =$ number of times m occurs in G
5. $p_m =$ probability that number of time occurrence of $m \geq c_m$
6. $p_r =$ already defined probability threshold for the occurrence of m
7. $h =$ isomorphic subgraph of g
8. $f =$ function defining that g has one to one correspondence with h
9. $l =$ search graph
10. $q =$ searching pattern corresponding to m
11. $H =$ property value for pattern searching
12. $domain(f) =$ corresponds to H
13. $n_j =$ individual nodes in graph
14. $N =$ set of nodes in graph
15. $k =$ threshold value signifying links

Algorithm

Feedback pattern identification
for each possible pattern m **do**
    let c_m is number of times m occurs in network graph G
    estimate $p_m = p_r[\#occ \geq c_m]$
    for each node in $g \epsilon G$ **do**
    for each node in $h \epsilon H$ **do**
    if h can't support g **then continue**
    let $f = \{(g \rightarrow h)\}$
    $l = Elaborate(f, g, h)$
    for q in l **do**
    output
    Elaborate(f, g, h)
    if $domain(f) = H$ **then**
    return $[f]$
    let m is some node in $N(domain(f))$
    for each node $n \epsilon N(f(domain(f)))$ **do**
    if adding $(m \rightarrow n)$ to f keeps f as a valid pattern, then
    Elaborate

Activation

$\forall\ n_j \epsilon N$

if $d^+(n_j \geq 2)$ **then**

if link **exists** between $(n_{j+1}(k), n_{j-1},(k))$ **then**
output

Calculate n_j if n_j increases with time

Inhibition

$\forall\ n_j \epsilon N$

if $d^+(n_j \geq 2)$ **then**

if link **exists** between $(n_{j+1}(k), n_{j-2}(k))$ **then**
output

Calculate n_j if n_j decreases with time

Monovalent link

$\forall\ n_j \epsilon N$

if $d^+(n_{j+1} \geq 2)$ **then**

if $d^+(n_{j+1}) == 1)$ **then**

if link **exists** between (n_{j+1}, n_{j-1}) **then**
Output: Monovalent link

Divalent link

$\forall\ n_j \epsilon N$

if $d^+(n_{j+1} \geq 2)$ **then**

if $d^+(n_{j+1}) > 1)$ **then**

if link **exists** between (n_{j+1}, n_{j-1}) **then**
Output: Divalent link

Iso-functional enzyme links

$\forall\ n_j \epsilon N$

if $d^+(n_{j+1} \geq 2)$ **and** link **exists** between (n_{j-1}, n_j) is ≥ 2
then

if $d^+(n_{j+1}) > 1)$ **then**

if link **exists** between $(n_{j+1}(k), n_{j-1}(k))$ **then**
Output: Iso-functional enzyme link

Sequential links

$\forall\ n_j \epsilon N$

if $d^+(n_{j+1} \geq 2)$ **then**

if link **exists** between $(n_j(k), n_{j-1}(k))$ **then**
Output: Sequential link

Concerted links

$\forall\ n_j \epsilon N$

if $d^+(n_{j+1} \geq 2)$ **then**

if link **exists** between $(n_j(k), n_j(k+1))$ **then**
Output: Concerted link

Cumulative links

$\forall\ n_j \epsilon N$

if $d^+(n_{j+1} \geq 2)$ **then**

if link **exists** between $(n_j(k), n_{j-1}(k))$ **or** between $(n_j(k+1), n_{j-1}(k))$ **or** between $(n_j(k), n_j(k+1), n_{j-1})$ **then**
Output: Cumulative link

The next Section deals with analyzing another important feature of metabolic pathway that is necessary for interpreting spread of infections, known as sensitivity, which is in continuation with our studies of feedback reactions.

Sensitivity analysis

Nesterov (1999) describes sensitivity analysis as 'the systematic investigation of the model responses to either perturbations of the model quantitative factors or variations in the model qualitative factors' [26]. Understanding sensitivities of metabolic pathways makes us chose those nodal points which are absolutely essential for growing the overall functioning of metabolic pathways. Sensitivities also help us to quantify the rate of change of the internal dynamics of the systems in metabolic pathways in response to external and internal perturbation, especially in case of external infection attack and spread. This section is described under two headings, namely, local sensitivity analysis and global sensitivity analysis.

Local sensitivity analysis. Local sensitivity analysis deals with considering changes to a single parameter at one time, by keeping others fixed. Consider a general ODE model of the form $\frac{dy}{dt} = f(y, k), y(0) = y^0$. Here, y is the vector of variables, k is the m-vector of system parameters and y^0 is the initial value. Thus, the effect of a small parameter change on the solution is expressed as a Taylor series expansion, $y_i(t, k + \Delta k) = y_i(t, k) + \sum_{j=1}^{m} \frac{\partial y_i}{\partial k_j} \Delta k_j + \frac{1}{2} \sum_{l=1}^{m} \sum_{j=1}^{m} \frac{\partial^2 y_i}{\partial k_l \partial k_j} \Delta k_l \Delta k_j + ...$ The partial derivatives $\frac{\partial y_i}{\partial k_j}$ are first-order local sensitivity coefficients and form the sensitivity matrix $S(t) = s_{ij} = \frac{\partial y_i}{k_j}$. In this case, $s_{ij}(t)$ describes the effect on the ith output variable at time t of a small change in the jth parameter around its nominal value.

Here, we used the finite-difference method for calculating the local sensitivities of the network. Using this method the model is solved at some chosen parameter point and then at some perturbed value of each parameter, $k_j + \Delta k_j$ while all other parameters are held at their nominal values. The sensitivities are then calculated using the finite-difference approximation method, $s_{ij}(t) \approx \frac{y_i(k_j + \Delta k_j, t) - y_i(k_j, t)}{\Delta k_j}$. Moreover, it assumes local linearity around a nominal parameter point [27].

Global sensitivity analysis. Global sensitivity analysis deals with considering changes to multiple parameters at one time. Here, we used Sobol's method for performing global sensitivity analysis. In this case, given a function $y = f(x)$ where y is output and x is a vector of k model input parameters, it can be represented in the form, $f(x) = f_0 + \sum_{s=1}^{n} \sum_{i_1 < ... < i}^{n} f_{i_1...i_s}(x_{i_1...i_s})$, where $1 \leq i_1 < ... < i_s \leq n$. This equation is called Analysis of Variance (ANOVA) representation of $f(x)$ if $\int_0^1 f_{i_1...i_s}(x_{i_1...i_s} dx_k = 0, k = i_1, ..., i_s$

Also, we can have, $\int f(x) dx = f_0$ $\int f(x) \Pi_{k \neq i} dx_k = f_0 + f_i(x_i)$ $\int f(x) \Pi_{k \neq i, j} dx_k = f_0 + f_i(x_i) + f_j(x_j) + f_{ij}(x_i, x_j)$ Thus, assuming that $f(x)$ is square integrable, then all the $f(i_1...i_s)$ are also square integrable. So, we have $\int f^2(x) dx - f_0^2 = \sum_{s=1}^{n} \sum_{i_1 < ... < i_s}^{n} \int f_{i_1 < ... < i_s}^2 dx_{i_1}...dx_{i_s}$

Thus, it is based on a decomposition of the variance term of increasing dimensionality. Furthermore, these partial variances are estimated using Monte-Carlo integrals and sensitivities are based on their ratio to total variances [28].

Damage analysis

The processes of infection and curing run for a specific number of iterations, depending on the number of metabolites in the metabolic pathway. We have assigned a maximum iteration value of $n/2$, where n is the total number of metabolites in the metabolic pathway [5]. The reason for this threshold is that after the iteration value is $n/2$, the results converge and there is no further need to continue performing further iterations. After the infection has been combated and number of iterations is completed, the critical value 'ρ_4', signifying the number of metabolites that cannot be cured, is calculated. Here, $\rho_4 = M - I'$, where M is network size and I' is the number cured metabolites. Three conditions can arise on the basis of calculating values of ρ_4. These are, ρ_4 *is* $\begin{cases} < 0 \\ = 0 \\ > 0 \end{cases}$

Here, $\rho_4 < 0$ indicates that there is a certain level of noise or external metabolites which are not cured in the metabolic pathway, $\rho_4 = 0$ explains that all infected metabolites are cured and size of the metabolic pathway remains unchanged, whereas $\rho_4 > 0$ specifies that some infected metabolites are not cured completely. Thus, it highlights whether the network is completely cured or not and also helps in analyzing those metabolites, which if infected cannot be restored back, predicting the damage done to the entire metabolic pathway [29]. Moreover, for full infection removal and curing, ρ_4 should always be 0.

Results

We demonstrated the effectiveness of our method on the metabolic pathways of *H. sapiens* for Type I *Diabetes mellitus* (T1D) involving GAS and INS genes. These metabolic pathways were that of glutamate metabolism, β-alanine metabolism, taurine and hypotaurine metabolism and butanoate metabolism. Our primary concern while working on this method was developing a framework which could be used to track the spread, prevalence and containment of any infection in normal healthy metabolic pathways of *H. sapiens*. The first step involved in this process is collecting datasets. For this reason, we searched for the metabolic pathway map of T1D for *H. sapiens* in KEGG. The genes which were explicitly involved in these pathways of *H. sapiens* (i.e., glutamate metabolism, β-alanine metabolism, taurine and hypotaurine metabolism, and butanoate metabolism) were GAD1, GAD2 and INS respectively. The remaining genes were involved in many other networks which were not directly involved in the causal mechanism of T1D. The next step of our data collection was identifying enzymes involved in these pathways relating to T1D. This was followed by searching the biochemical reactions catalyzed by these enzymes, involved in the metabolic pathways relating to T1D. This section is described under six headings, namely, modeling metabolic pathways quantitatively, modeling infection spread in metabolic pathways, detecting feedback reactions in metabolic pathways, performing local sensitivity analysis, performing global sensitivity analysis and analyzing the damage caused in metabolic pathways due to infection spread.

Modeling metabolic pathways quantitatively

As discussed in section 'Methodology', we used ODEs to quantitatively model the four metabolic pathways involved in the functioning of GAD and INS genes in T1D. This ODE model of glutamate metabolism was already discussed in section 'Methodology'. Here, we discuss the ODE formulation of the other three metabolic pathways. The ODE representation of these pathways is present in Section S1 in File S1. For simplification purpose, the initial values of all the kinetic parameters as well as other entities, like metabolites were assumed to be $1\,\mu M$ [8]. For initializing the functioning of all the reactions, the default volume, V_{def} was taken into consideration. Section S1(SI) in File S1 represent the reactions present in β-alanine metabolism, consisting of 17 reactions in total. Here, $a...q$ represent the genes involved in various reactions. The various kinetic parameters for reactions 1 to 17 are $k1-rn1-a$, $k1-rn2-b$, $k1-rn3-c$, $k1-rn4-d$, $k1-rn5-e$, $k1-rn6-f$, $k1-rn7-g$, $k1-rn8-h$, $k1-rn9-i$, $k1-rn10-j$, $k1-rn11-k$, $k1-rn12-l$, $k1-rn13-m$, $k1-rn14-n$, $k1-rn15-o$, $k1-rn16-p$ and $k1-rn17-q$ respectively. Furthermore, the kinetic parameters involved in the ODEs were different for various metabolites. For instance, in β-alanine metabolism, $malonyl-CoA$ had kinetic parameters $k1-rn1-a$ and $k1-rn3-c$, $acetyl-CoA$ had kinetic parameters $k1-rn3-c$ and $k1-rn1-a$, $L-aspartate$ had

$k1-rn2-b$, $\beta-alanine$ had $k1-rn5-e$, $k1-rn6-f$, $k1-rn8-h$, $k1-rn11-k$, $k1-rn2-b$, $k1-rn4-d$, $k1-rn7-g$, $k1-rn12-l$, $k1-rn16-q$, $malonate$ had $k1-rn3-c$, $acetate$ had $k1-rn3-c$, $3-ureidopropionate$ had $k1-rn4-d$, $k1-rn13-m$, $2-oxoglutarate$ had $k1-rn5-e$, $3-oxopropanoate$ had $k1-rn5-e$, $L-lysine$ had $k1-rn6-f$, $k1-rn7-g$, $\beta-alanyl-L-lysine$ had $k1-rn7-g$, $k1-rn6-f$, $L-arginine$ had $k1-rn8-h$, $\beta-analyl-L-arginine$ had $k1-rn17-g$, $k1-rn8-h$, $5,6-dihydrouracil$ had $k1-rn9-i$, $k1-rn10-j$, $k1-rn13-m$, $uracil$ had $k1-rn9-i$, $k1-rn10-j$, $L-histidine$ had $k1-rn12-l$, $k1-rn11-k$, $carnosine$ had $k1-rn11-k$, $k1-rn12-l$, $S-adnosyl-methioniamine$ had $k1-rn14-n$, $spermidine$ had $k1-rn14-n$, $5'-methyl-thioadenosine$ had $k1-rn14-n$, $3-hydroxypropionyl-CoA$ had $k1-rn16-p$, $k1-rn15-o$, $propenoyl-CoA$ had $k1-rn15-0$ and $3-hydroxypropanoate$ had $k1-rn16-p$ respectively.

Similarly, taurine and hypotaurine had 6 reactions (Section S1(SII) in File S1) with $3-sulfinoalanine$ having kinetic parameters $k3-rn1-a$, $k3-rn2-b$, $hypotaurine$ had $k3-rn3-c$, $k3-rn1-a$, $3-cysteamine$ had $k3-rn3-c$, $3-cysteine$ had $k3-rn2-b$, $taurine$ had $k3-rn1-a$, $k3-rn5-e$, $k3-rn4-d$, $L-cysteate$ had $k3-rn1-a$, $glutaurine$ had $k3-rn5-e$, $taurocholate$ had $k3-rn4-d$, $5-L-glutaryl-peptide$ had $k3-rn5-e$, $choloyl-CoA$ had $k3-rn4-d$ and CoA had $k3-rn4-d$ respectively. The reason for explicitly defining these kinetic parameters was that these change in accordance with the concentration of metabolites with respect to time, which plays a pivotal role for the overall functioning of the metabolic pathways.

Lastly, butanoate metabolism had 15 reactions (Section S1(SIII) in File S1)with the metabolite $pyruvate$ having kinetic parameters $k2-rn1-a$, $thiaminediphosphate$ had $k2-rn1-a$, $2\alpha-hydroxyethyl-thiamino-diphosphate$ had $k2-rn1-a$, $acetyl-CoA$ had $k2-rn9-i$, $k2-rn13-m$, $k2-rn2-6$, $acetoacetylCoA$ had $k2-rn2-b$, $k2-rn4-d$, $k2-rn8-h$, $k2-rn12-l$, $k2-rn13-m$, $L-glutamate$ had $k2-rn11-k$, $k2-rn3-c$, $4-aminobutanoate$ had $k2-rn3-c$, $k2-rn11-k$, $succinylCoA$ had $k2-rn4-d$, $acetoacetate$ had $k2-rn9-i$, $k2-rn10-j$, $k2-rn4-d$, $k2-rn8-h$, $succinate$ had $k2-rn14-h$, $k2-rn5-e$, $succinatesemialdehyde$ had $k2-rn11-k$, $k2-rn5-e$, $butanoylCoA$ had $k2-rn7-g$, $k2-rn6-f$, $crotonoylCoA$ had $k2-rn6-f$, $k2-rn14-n$, $butanoicacid$ had $k2-rn7-g$, $(S)-3-hydroxy-3-methyl-glutaryl-CoA$ had $k2-rn9-i$, $k2-rn13-m$, $(R)-3-hydroxy-butanoate$ had $k2-rn10-j$, $2-oxoglutarate$ had $k2-rn15-o$, $k2-rn11-k$, $(R)-3-hydroxy-butanoyl-CoA$ had $k2-rn12-l$, $k2-rn14-n$ and $2-hydroxy-glutarate$ had $k2-rn15-o$ respectively [8,30].

For validation purpose, two strategies were considered, *first*, simulating the model with step changes in input dataset as well as in time series, and *second*, comparing the predicted output with published results [31]. For the first strategy, we started with initial concentration of all the metabolites and performed two perturbations, *first*, where we progressively reduced the concentration, and *second*, where we progressively increased the concentration of the metabolites (Section G in File S1) [31,32]. For instance, for analysing the rate of change of $malonyl-CoA$ in β-alanine metabolism, with initial concentration of $0.4\,\mu M/ml$, $acetyl-CoA$ ($0.3\,\mu M/ml$), $malonate$ ($0.2\,\mu M/ml$) and $acetate$ ($0.2\,\mu M/ml$), $\frac{d}{dt}([malonyl-CoA].V_{def}) = -0.88$ (keeping $V_{def} = 1\,\mu l$, $[a] = 1$, $[c] = 1$). Similarly, for 1st metabolite, $\frac{d}{dt}([malonyl-CoA].V_{def}) = -0.38$, 2nd metabolite,

$\frac{d}{dt}([malonyl-CoA].V_{def})=-0.29$, 3rd metabolite, $\frac{d}{dt}([malonyl-CoA].V_{def})=-1.12$ and 4th metabolite, $\frac{d}{dt}([malonyl-CoA].V_{def})=-0.45$ respectively. We observed that with decrease in concentration of $malonyl-CoA$, $\frac{d}{dt}([malonyl-CoA].V_{def})$ increased, whereas it decreased further when concentration was increased by $0.1\,\mu M/ml$ and again increased when concentration was increased by $0.1\,\mu M/ml$. Thus, we could observe that decreasing concentration increased the rate of change and vice versa, which is predictable from the ODEs [33,34].

Next, using the 2nd validation strategy, we found that for $\beta-alanine$ metabolism, it has been seen that when $malonyl-CoA$ function is altered in cells, *glucose*-induced insulin release is impaired. Furthermore, it is already known that citrate, exported from mitochondria to the cytosol, is cleaved by ATP citrate lyase, forming *oxaloacetate* and *acetyl-CoA*, which form $malonyl-CoA$ promoting fatty acid synthesis, accumulating long-chain $acetyl-CoA$ enhancing Ca^{2+} evoked insulin exocytosis. Thus, it proved the importance of $malonyl-CoA$ as determined by our algorithm [35–37].

Modeling infection spread in metabolic pathways

The fundamental aspect of analyzing the infection spread is selecting the infection starting point. There are two methods for such selection, namely, random and targeted [5]. Random method is selecting any metabolite as infection start site without any bias. But, this does not help in disease study. The reason being, based on literature and experimental evidences, some known metabolites participating in T1D is already known. Thus, we concentrate on targeted selection, which specifically selects metabolites based on our choice (Table 1). We start our discussion with *glutamate* metabolism, having 15 metabolites, namely, $N-carbamoyl-L-aspartate(1),L-glutamine(2),$ $L-glutamate(3),4-aminobutanoate(4),ammonia(5),$ $5-phosphoribosylamine(6),D-glucosamine6-phosphate(7),$ $D-fructose-6-phosphate(8),2-oxoglutarate(9),$ $2-oxoglutaramte(10),succinatesemialdehyde(11),5-phospho-$ $\alpha-D-ribose-1-diphosphate(12),L-glutamate-5-$ $semialdehyde(13),L-aspartate(14)$ and $succinate(15)$ (Table 2). The numbers in bracket represent a metabolite. In *glutamate* metabolism, the selected start sites for infection spread are $L-glutamate(3)$ and $4-aminobutanoate(4)$ respectively. Initially, in infection-free state, $M=14,N=0,P=0,I_{act}=0$ and $I'=0$. We executed our simulation algorithm by considering 3 as the start site of infection initiation in the 1st run (Fig. S1 in File S1). The front propagation of 3, $d^{+}(3)=5$ as it was connected to five metabolites, namely, 4,2,17,9, and 8. The burning probability of 3,$BP(3)=0.2$, stating the fact that the chance of infection spread to the five connected metabolites was 3, i.e., 20% each. Similarly for metabolite 4,$d^{+}(4)=1$, as it was connected to only one metabolite, i.e. 11, whereas the burning probability, $BP(4)=1$, suggesting that the chance that metabolite 11 would be infected was very high (100%). Next the front propagation of 5,$d^{+}(2)=5$, as it was connected to five metabolites, namely, 7,13,14,15, and 20 whereas its burning probability, $BP(2)=0.2$, again suggesting the fact that chance of infection spread through 2 is 20%. Furthermore, for metabolites 17 and 9, the front propagation values are $d^{+}(17)=0$ and $d^{+}(9)=0$, suggesting that they had no possibility of infection spread through them. For metabolite 8, the front propagation, $d^{+}(8)=1$, as it was connected to only one metabolite, namely, 10 and had a burning probability, $BP(8)=0.5$, having 50% chance that infection would spread through it. Similarly for metabolite 7, the front propagation,

$d^{+}(7)=1$, as it is connected to one metabolite, i.e. 16, whereas its burning probability, $BP(7)=0.5$. Furthermore, front propagation value of metabolite 10,$d^{+}(10)=1$, as it is connected to one metabolite, i.e., 18 and had a burning probability, $BP(10)=0.5$. Moreover, front propagation value for other metabolites 16,13,14,15,20,17,9 and 18 was 0 suggesting no infection spread through these metabolites (Fig. 4).

As this simulation had been done only on the basis of structural aspects of the network, biological significance needs to be associated with this model. For this purpose, we calculated certain quantitative parameters associated with it. Thus, for $L-glutamine,M=14,N=0,P=4,I_{act}=7,I_{pas}=4,$ $N_{p}=0,C_{act}=\frac{1}{I_{act}}=0.14,C_{pas}=\frac{1}{I_{pas}}=0.25,I=14,$ and $I'=14.$ $q=0,\beta=0,\alpha=1,\mu=\frac{P}{M}=0.28,\epsilon=0$

Similarly, we observed that $\frac{dP}{dt}=-13.14,\frac{dI_{act}}{dt}=389.88,$ $\frac{I_{pas}}{dt}=0.08,\rho_{4}=M-P'=0.$ Thus, the critical factor, $\rho_{4}=0$, even after selecting $L-glutamate$ as infection start site. For the 2nd run, we selected metabolite 4 as start site for infection spread (Fig. S in File S1). It had a front propagation, $d^{+}(4)=1$, as it was connected to 11, and had a burning probability $BP(4)=1$, suggesting the chance of infection spread as 100%. Continuing the same strategy, we found that for metabolite 11, the front propagation, $d^{+}(11)=1$, as it was connected to 19. Furthermore, for 11 and 19, the burning probability values were $BP(11)=1$ and $d^{+}(19)=0$ suggesting the termination of infection spread (Fig. 5). A combat mechanism also occured simultaneously along with infection spread. For instance, when 3 got infected, 12 acted in accordance that results in healthy production of 3. The reason being, back propagation of metabolite 3,$d^{-}(3)=1$ and its combating probability, $CP(3)=1$, demonstrating the fact that even if it got infected combating the infection occurred. In this case, the combating edge was in between metabolites 3 and 12 (Fig. S3 in File S1). In case of metabolite 4,$d^{-}=1,CP=1$ was selected as the start site for infection, 3 acted in accordance to combat the infection. Thus, the combating edge was in between 3 and 4 respectively (Fig. S4 in File S1). Now, for $v_{i}=4(4-aminobutanoate),M=14,N=0,P=1,I_{act}=2,I_{pas}=1,$ $N_{p}=0,C_{act}=0.5,C_{pas}=1,I=14,q=0,\beta=0,\alpha=1,\mu=0.07,\epsilon=0$ and $I'=14.$ Thus, $\frac{dP}{dt}=13.93,\frac{dI_{act}}{dt}=95.88,\frac{I_{pas}}{dt}=0.86,\rho_{4}=0.$ Thus, selecting $4-aminobutanoate$ again gave 0 as critical factor.

In case of $\beta-alanine$ metabolism, two runs were possible as only two possible metabolites, $\beta-alanine$ and $L-aspartate$ acted as possible start sites for infection. Selecting $\beta-alanine(d^{+}=3,BP=0.33)$ as start site results in infecting 3 metabolites, namely, $\beta-alanyl-N-pi-methyl-L-histidine$ $(d^{+}=0),\beta-amino-propion-aldehyde(d^{+}=1,BP=1),$ and $3-oxopropanoate(d^{+}=0).$ The metabolite $3-oxopropanoate$ infected $1,3-diaminopropane(d^{+}=0)$ resulting in no further infection progress (Section S2 Fig. S6 in File S1). Now, for biological significance and validation purpose,we found that $M=25,N=0,P=2,I_{act}=4,I_{pas}=2,N_{p}=0,C_{act}=0.25,$ and $C_{pas}=0.5,I=25,q=0,\beta=0,\alpha=1,\mu=0.28,\epsilon=0$ $I'=25.$ Thus, $\frac{dP}{dt}=18.84,\frac{dI_{act}}{dt}=198.84,\frac{I_{pas}}{dt}=-1.32,\rho_{4}=0.$ We observed that critical factor was *zero* using ODE, confirming our previous analysis using graph-based study. It is also known from literature that altering the level of $\beta-alanine$ may affect the formation of *carnosine* in cells resulting in several side effects

Table 1. Initiating metabolites for Type I *Diabetes mellitus* in *H. sapiens*.

Metabolic pathway	Infection start site	Number of connecting links	Reaction links
Glutamate metabolism	L-glutamate	05	L-glutamate→4-aminobutanoate
			L-glutamate→ρ_4-L-glutanyl-L-cysteine
			L-glutamate→L-glutamyl-tRNA Glu
			L-glutamate→L-glutamine
			L-glutamate→2-oxoglutarate
	4-aminobutanoate	02	4-aminobutanoate→succinate semialdehyde
			4-aminobutanoate→L-glutamate
β-alanine metabolism	β-alanine	05	β-alanine→*beta*-alanyl-N-pi-methyl-L-histidine
			β-alanine→L-aspartate
			β-alanine→3-ureidopropionate
			β-alanine→*beta*-aminopropion aldehyde
			β-alanine→3-oxopropanoate
	L-aspartate	01	L-aspartate→*beta*-alanine
Taurine and hypotaurine metabolism	3-sulfino-L-alanine	02	3-sulfino-L-alanine→hypotaurine
			3-sulfino-L-alanine→L-cysteine
	Taurine	03	Taurine→taurocholate
			Taurine→L-cysteate
			Taurine→5-glutamyl-taurine
	L-cysteate	01	L-cysteate→taurine
	Hypotaurine	02	Hypotaurine→3-sulfino-L-alanine
			Hypotaurine→cysteamine
Butanoate metabolism	4-aminobutanoate	02	4-aminobutanoate→succinate semialdehyde
			4-aminobutanoate→L-glutamate
	L-glutamate	01	L-glutamate→4-aminobutanoate

such as reduction in antioxidant level as well as other carbohydrate-based disorders [38,39]. In case of combat operation, initiating with $\beta-alanine metabolism, \beta-alanine(d^- =2,CP=0.5)$ had two possible combating edges with metabolites $3-ureidopropionate$ and $L-aspartate$ respectively (Section S2 Fig. S7 in File S1) [17]. Furthermore, L-aspartate $(d^- =1, CP=1)$ has only one possible combating edge with metabolite 3-ureidopropionate (Section S2 Fig. S8 in File S1). Furthermore, selecting $L-aspartate(d^+ =1,BP=1)$ as infection spread infects only $\beta-alanine$, which further spreads the infection (as discussed previously) (Section S2 Fig. S9 in File S1). Also, $M=25,N=0,P=1,I_{act}=1,I_{pas}=4,N_p=0,C_{act}=1,C_{pas}=0.25,$ $I=25,q=0,\beta=0,\alpha=1,\mu=0.08,\epsilon=0,I'=24$. Thus, $\frac{dP}{dt}=18.68,$ $\frac{dI_{act}}{dt}=98.68, \frac{I_{pas}}{dt}=-1.08, \rho_4=1$, with critical factor as non-zero, thus having possibility for infection spread through metabolite. From literature, it is known that $L-aspartate$ is essential for metabolic demand and is categorized as an important precursor for $\beta-alanine$, thereby significantly participating in insulin functioning [40,41].

Furthermore, in $taurine-hypotaurine$ metabolism, four runs were possible as $3-sulfino-L-alanine, taurine, L-cysteine$ and $hypotaurine$ could act as start site. For the 1st run, when $3-sulfino-L-alanine(d^+ =2,BP=0.5)$ acted as the start site, it infects $hypotaurine(d^+ =0)$ and $L-cysteine(d^+ =0)$ resulting in no further progress (Section S2 Fig. S10 in File S1). Here,

$M=11,N=0,P=1,I_{act}=1,I_{pas}=1,N_p=0,C_{act}=1,C_{pas}=1,$ $I=11,q=0,\beta=0,\alpha=1,\mu=0.09,\epsilon=0,I'=11$. Thus, $\frac{dP}{dt}=13.68, \frac{dI_{act}}{dt}=9.91, \frac{I_{pas}}{dt}=-1.09$. We have found that the fact $\rho_4=0$ validates our result. From literature, we found that $L-cysteine$ inhibits insulin release from pancreatic β-cell, thereby playing a significant role [42,43]. This proved our previous conclusion that selecting $3-sulfino-L-alanine$ infected $L-cysteine$ which might further effect the production of insulin [42]. Meanwhile, in $taurine-hypotaurine$ metabolism, $3-sulfino-L-alanine(d^- =1,CP=1)$ had only one possible combat edge with $L-cysteine$. Moreover, if $taurine(d^+ =2,BP=0.5)$ was selected as start site (for the 2nd run), it infected $5-glutamyl-taurine(d^+ =0)$ and $taurocholate(d^+ =0)$ resulting in no more infection spread (Section S2 Fig. S11 in File S1) [44]. Now, $M=11,N=0,P=2,I_{act}=2,I_{pas}=2,N_p=0,C_{act}=0.5,C_{pas}=0.5,$ $I=11,q=0,\beta=0,\alpha=1,\mu=0.18,\epsilon=0,I'=11$. Thus, $\frac{dP}{dt}=11.91,$ $\frac{dI_{act}}{dt}=43.64, \frac{I_{pas}}{dt}=-1.36, \rho_4=0$. Also, $taurine(d^- =1,CP=1)$ had a combat edge with $L-cysteate(d^- =0)$ which had no further mechanism of combat (Section S2 Figs. S12–S14 in File S1) [45]. Similarly for the 3rd run, when $L-cysteate(d^+ =1,BP=1)$ acted as start site, it infects taurine resulting in further infection spread (as discussed previously)(Section S2 Fig. S15 in File S1), for which $M=11,N=0,P=2,$

Table 2. Reactions and metabolites involved in glutamate metabolism in *H. sapiens*.

Reactions
$Succinatesemialdehyde + NAD+ + H_2O <=> Succinate + NADH + H^+; [y],[rn1]$
$4-Aminobutanoate + 2-Oxoglutarate <=> Succinatesemialdehyde + L-Glutamate; [x],[rn2]$
$L-Glutamate <=> 4-Aminobutanoate + CO_2; [z],[rn3]$
$L-Glutamate + NAD+ + H_2O <=> 2-Oxoglutarate + NH_3 + NADH + H^+; [a],[rn4]$
$2-Oxoglutaramate + H_2O <=> 2-Oxoglutarate + NH_3; [f],[rn5]$
$L-Glutamine + D-Fructose6-phosphate <=> L-Glutamate + D-Glucosamine-6-phosphate; [b],[rn6]$
$5-Phosphoribosylamine + Diphosphate + L-Glutamate <=> L-Glutamine + 5-Phospho-alpha-D-ribose-1-diphosphate + H_2O; [g],[rn7]$
$ATP + L-Glutamate + NH_3 <=> ADP + Orthophosphate + L-Glutamine; [h],[rn8]$
$L-Glutamine + H_2O <=> L-Glutamate + NH_3; [c],[rn9]$
$L-Glutamate5-semialdehyde + NAD^+ + H_2O <=> L-Glutamate + NADH + H^+; [d],[rn10]$
$2ATP + NH_3 + CO_2 + H_2O <=> 2ADP + Orthophosphate + Carbamoylphosphate; [p][rn11]$
$Carbamoylphosphate + L-Aspartate <=> Orthophosphate + N-Carbamoyl-L-aspartate; [i],[rn12]$

doi:10.1371/journal.pone.0069724.t002

$I_{act} = 2, I_{pas} = 2, N_p = 0, C_{act} = 0.5, C_{pas} = 0.5, I = 11, q = 0, \beta = 0,$
$\alpha = 1, \mu = 0.18, \epsilon = 0, I' = 11.$ Thus, $\frac{dP}{dt} = 11.91, \frac{dI_{act}}{dt} = 43.64,$
$\frac{I_{pas}}{dt} = -1.36, \rho_4 = 3.$ We observed that critical factor was high in this case, thus validating our result again. $L-cysteate$ had been found to be important in synthesis of various other metabolites like *taurine*, which plays an essential role in improving insulin resistance [46,47]. As per our finding, infecting taurine may drastically spread this infection throughout. Lastly for the 4th run, selecting $hypotaurine(d^+ = 0)$ did not result in any further progress of infection (Section S2 Fig. S16 in File S1) [45]. In this case, $M = 11, N = 0, P = 0, I_{act} = 0, I_{pas} = 0, N_p = 0, C_{act} = 0,$
$C_{pas} = 0, I = 0, q = 0, \beta = 0, \alpha = 0, \mu = 0.0, \epsilon = 0, I' = 1.$
Thus, $\frac{dP}{dt} = 0, \frac{dI_{act}}{dt} = 0, \frac{I_{pas}}{dt} = 0, \rho_4 = 3$ [48]. Results on Infection spread analysis in butanoate metabolism has been discussed in Section S2 Figs. S17–S20 in File S1.

Detecting feedback reactions in metabolic pathways

Here, we discuss the results that we got by identifying the presence of feedbacks in the above mentioned four metabolic pathways. We performed the analysis in two steps. First, we identified the presence of a feedback pattern using the algorithm discussed in section 'Methodology', and second, we validated this property biologically using the notation previously discussed in section 'Analyzing feedbacks'. For glutamate metabolism, we found the presence of three possible feedback links (all sequential links), in the form of reactions $L-glutamate \rightarrow 2-oxoglutarate,$ $L-glutamate \rightarrow L-glutamine$ and $L-glutamine \rightarrow L-glutamate$ respectively (Section S3 Fig. S21a in File S1). This detection was performed on the basics of 'Sequential Links' algorithm in section 'Methodology'. Thus, $d^+(n_{j+1}) = 5$ ($L-glutamate$), $d^+(n_{j+1}) = 6$ ($L-glutamine$) and $d^+(n_{j+1}) = 2$ (*oxoglutarate*). Now, for $k = 1,$ links exist between $2-oxoglutarate, L-glutamate$ and $L-glutamine$ respectively. For the other feedback categories, meaningful results did not exist. For validation, we found $\frac{dx_1}{dt}$ for $L-glutamate$ and $L-glutamine$, whereas $\frac{dx_2}{dt}$ for $2-oxoglutarate$ and $L-glutamine$. Thus, for initial concentration of 1 μM for all the

metabolites, $\frac{dx_1}{dt}$ for $L-glutamate = -\frac{a_1 x_1}{(k_1 + x_1)(1 + \alpha . x_n)} - \phi . x_1 - c = 1$ and $\frac{dx_1}{dt}$ for $L-glutamine = 1,$ whereas $\frac{dx_2}{dt}$ for $2-oxoglutarate = -\frac{a_1 x_1}{(k_1 + x_1)(1 + \alpha . x_n)} - \frac{a_2 x_2}{(k_2 + x_2)} - \phi . x_2 = 0.05$ and $\frac{dx_2}{dt}$ for $L-glutamaine = 0.01$ respectively [49,50]. Thus, with time, the concentration of $2-oxoglutarate, L-glutamine$ and $L-glutamate$ follows a negative downgrade, making the reactions behaved in a feedback manner [9,50].

Similarly, for $\beta-alanine$ metabolism, only one reaction displayed properties of feedback, namely, $acetyl-CoA + malonate \leftrightarrow acetate + malonyl-CoA$, where sequential link is established. Thus, $d^+(n_{j+1}) = 2$ ($acetyl-CoA$). Now, for $k = 1,$ links existed between $acetyl-CoA$ and $malonyl-CoA$. For the purpose of validation, we found that $\frac{dx_1}{dt}$ for $acetyl-CoA = 1$ and $\frac{dx_2}{dt}$ for $malonyl-CoA = 0.02$. Furthermore, concentration of $malonyl-CoA$ decreases with time (Section S3 Fig. S21b in File S1) [49]. In case of $taurine-hypotaurine$ metabolism, sequential link was established in two reactions, namely, $3-sulfinoalanine \rightarrow hypotaurine$ and $taurine + (5-L-glutaryl) -peptide \rightarrow glutaurine + peptide$. For $d^+(n_{j+1}) = 2$ (*sulfinoalanine*) and $d^+(n_{j+1}) = 4$ (*taurine*) and $k = 1,$ links were present between $3-sulfinoalanine, hypotaurine, taurine$ and $5-glutaryltaurine$ [51,52]. Thus, for the purpose of validation, we found, $\frac{dx_1}{dt}$ for $3-sulfinoalanine = 1,$ $\frac{dx_2}{dt}$ for $hypotaurine = -2.39E-30,$ $\frac{dx_1}{dt}$ for $taurine = 1,$ $\frac{dx_2}{dt}$ for $5-glutaryltaurine = 0.28,$ where concentration of *hypotaurine* decreased with time whereas that of *taurine* increased (Section S3 Fig. S21c in File S1) [9,45]. Results on feedback detection in butanoate metabolism has been discussed in Section S3 Fig. S21d in File S1.

Performing local sensitivity analysis

Every reaction model of metabolic pathways contain a number of parameters like initial concentration of metabolites and kinetic constants, whose values are not known exactly. Altering these parameters change the behavior of the model, and also specify

Table 3. Representing values corresponding to local sensitivity analysis done on glutamate metabolism; rows signify fluxes and columns denote the metabolites participating in various reactions.

Reaction ID	Flux ID (rn:)	L-glut amate	L-glut amine	4-amino butan oate	5-phos phorib osylam ine	D-gluc osami ne-6P	succ inate semial dehyde	succ inate	2-oxo gluta rate	2-oxo glutar amate	D-fruc tose 6P	5-P-α-D ribose 1-diP	L-glutam ate-5 semial dehyde	L-asp art ate
y	(1)	0	0	0	0	0	0.023467	1.98E-18	0	0	0	0	0	0
x	(2)	0	0	0.012564	0	0	2.03E-20	0	0.054354	0	0	0	0	0
z	(3)	0	0.015343	1.23E-21	0	0	0	0	0	0	0	0	0	0
a	(4)	0	0	0	0	0	0	0	2.10E-20	0	0	0	0	0
f	(5)	0	0	0	0	0	0	0	1.30E-21	0.067803	0	0	0	0
b	(6)	1.21E-20	1.80E-21	0	0	1.23E-21	0	0	0	0	0.189356	0	0	0
g	(7)	2.30E-20	0	0	1.18E-19	0	0	0	0	0	0	1.23E-18	0	0
h	(8)	0.185643	0	0	0	0	0	0	0	0	0	0	0	0
c	(9)	2.41E-19	1.20E-18	0	0	0	0	0	0	0	0	0	0	0
d	(10)	0	1.18E-19	0	0	0	0	0	0	0	0	0	0.198234	0
i	(11)	0	0	0	0	0	0	0	0	0	0	0	0	0.023876

doi:10.1371/journal.pone.0069724.t003

whether the model is dependent on these parameters or not. This is extremely essential in disease networks, as a right combination of parameters can be used to analyze the dynamics of the network. Local sensitivity analysis describes how much does a specific parameter change the behavior of the model. We have calculated the sensitivity values for different parameters based upon time courses using the finite-difference method (already discussed in section 'Methodology'). Here, we have performed sensitivity analysis using three different conditions, namely, concentration fluxes of reactions with initial concentrations, non-constant concentration of species with initial concentrations, and concentration rates with initial concentrations [27].

The sensitivities of all parameters with respect to all reactions in the model has been calculated and displayed in Table 3 where the columns correspond to the parameters (both metabolites and kinetic constants) and rows to the reactions. Let us consider the line labeled '(rn:R4).Flux' (Table 3), where the numbers described how the flux of reaction '(rn:R4).Flux' $(L-glutamate+NAD^++H_2O<=>2-oxoglutarate+NH^3+NADH+H^+)$ changed with concentrations of different parameters. Here, $L-glutamate$ is a substrate with initial concentration $1\,\mu M$ and $2-oxoglutarate$, a product showing negative gradient with concentration of $\approx -2.10E-20\,\mu M$, leading to a lower flux, which might ultimately lead to the decrease in reaction rate [27]. A sensitivity value equal to zero indicates that the metabolite concentration has no influence on the reaction rate. It is also important to know that sensitivity values are dominated by changes in enzyme concentrations, as they only measure the effects of changing the overall rate of reactions. Similarly, for the reaction flux, '(rn:R6).Flux', $(L-glutamine+D-fructose6-phosphate<=>L-glutamate+D-glucosamine6-phosphate)$, concentration of the reactant $(L-glutamine \approx -1.8E-21\,\mu M)$ decreased, as well as for reaction flux, '(rn:R7).Flux', $(5-phosphoribosylamine+Diphosphate+L-glutamate<=>L-glutamine+5-phospho-\alpha-D-ribose1-diphosphate+H_2O)$, where concentration of the reactant $(L-glutamate \approx -2.3E-20\,\mu M)$ decreased too, indicating positive correlation and normal reaction rate. Furthermore, values corresponding to non-constant concentration of species with initial concentrations, negative gradients has been indicated in case of metabolites $L-$ glutamate $\approx -2.27E-20\,\mu M$, $L-glutamine -1.7E-20\,\mu M$ and $2-oxoglutarate -1.8E-20\,\mu M$ for genes a, b and f respectively. Lastly, in Table 3 concentration rates with initial concentrations did not provide any meaningful result as values were 0 [51].

Validating the above sensitivity output with the already generated fire spread result on glutamate metabolism gave us some interesting conclusions. Selecting $L-glutamine$ as infection initiation site led to $\rho_4=0$ (Section S4 Table S1 in File S1). It suggested that though infection initiated at this site, all infected metabolites were ultimately cured. Furthermore, performing local sensitivity analysis indicated that concentration of infected $L-glutamine$ decreased with time suggesting the fact that since there was no negative flux associated with it, all infected metabolites were cured and glutamate metabolism functioning was not affected [27]. Similarly, for $\beta-alanine$ metabolism, in case of reaction flux '(rn:R000003).Flux', $(Acetyl-CoA+Malonate<=>Acetate+Malonyl-CoA)$ (Section S4 Table S2 in File S1), concentration of $malonyl-CoA \approx -1.67E-21\,\mu M$ decreased, that suggested that product concentration decreased with time, signifying its possible role to act in accordance with $malonyl-CoA$. Similarly, concentration of both $malonyl-CoA, acetate$ had a negative gradient values corresponding to non-constant concentration of selected metabolites [53]. Furthermore, we also observed that concentration of $\beta-alanine$, selected as infection initiation site decreased beyond $1.2E-21\,\mu M$. Also, concentration of $L-aspartate$ decreased beyond $0.189456\,\mu M$ in a manner supported by common enzymatic reaction [53,54].

Moreover, in case of $taurine-hypotaurine$ metabolism, the reaction flux '(rn:R02466).Flux', $(3-sulfinoalanine<=>hypotaurine+CO_2)$ (Section S4 Table S3 in File S1) has $hypotaurine \approx -2.39E-30\,\mu M$ decreasing in negative gradient suggesting a possible role in inhibition. Similarly, in reaction flux, '(rn:R01687).Flux', $(Taurine+5-L-glutaryl-peptide<=>Glutaurine+peptide)$ (Section S4 Table S3 in File S1), $taurine \approx 3.79E-36\,\mu M$ had a positive gradient. Now, in (Section S4 Table S3 in File S1), with non-constant concentration of species with respect to initial concentration displayed a negative gradient for $3-sulfinoalanine$ with $CDO1$ as gene. We observed that

concentration of $3-sulfinoanaline$ had a positive gradient even after $8.23E-31\,\mu M$ and did not give rise to non-zero critical factor [49,55]. But, selecting $L-cysteate$ had a non-zero critical factor, which could be clearly identified using its concentration values of $0\,\mu M, -5.7E-31\,\mu M, -5.75E-31\,\mu M, 1.72E-30\,\mu M$, $3.79E-36\,\mu M, -3.78E-36\,\mu M$, suggesting its possible role in inhibiting the reaction rate [27,51]. In this section we looked into the metabolic pathways from a local structure point of view, which suffers from several disadvantages such as, their role to investigate the model behavior in the immediate region around the nominal parameter values and only consider changes to one parameter at a time, while all other parameters are fixed to their nominal values. Thus, to understand this situation, we performed global sensitivity analysis of infected metabolic pathways [55]. Local sensitivity analysis results on butanoate metabolism has been discussed in Section S4 Table S4 in File S1.

Performing global sensitivity analysis

We have discussed previously that local sensitivity analysis considers changes to one parameter at a time, whereas in biological systems multiple parameters might act together to produce an effect. Thus, in a diseased network like T1D, it is extremely important to understand the role of multiple parameters in causing the disorder. For the same purpose, we implemented Sobol's method of global sensitivity analysis [28]. We have restricted ourselves to analyzing only those metabolites that we selected as infection start sites. We have studied the effect of metabolites upon one another, analyzing them individually as well as in groups of one, two, three and more at a time. For instance, in case of $glutamate$ metabolism, we selected four metabolites, namely, $2-oxoglutarate$, $4-aminobutanoate$, $L-glutamate$ and $L-glutamine$. In the 1st run, we studied the effect of $2-oxoglutarate$ over others, $4-aminobutanoate$ over others and so on. In the 2nd run, we studied in groups of two, like effect of $2-oxoglutarate$ and $4-aminobutanoate$ over others and so on. In the 3rd run, we studied in groups of three, whereas, in the 4th run, we studied the effect of metabolites in groups of four. Thus, we could validate our forest fire hypothesis and studied whether the effects of these metabolites as proposed in the fire spread model are true or not. Thus, for $2-oxoglutarate$, we found its maximal effect on $L-glutamate$, whereas for $4-aminobutanoate$, the maximal effect was found on $succinatesemialdehyde$, followed by $L-glutamine$ and $L-glutamate$. Similarly for $L-glutamate$, the maximal effect produced on $4-aminobutanoate$, followed by $L-glutamine$ and $2-oxoglutarate$, whereas for $L-glutamine$ the maximal effect was on $L-glutamate$ respectively (Figs. 7a–c) [56,57].

Considering two metabolites at a time, for $L-glutamate$ and $2-oxoglutarate$, maximal group effect was on $L-aspartate$, whereas for $L-glutamine$ and $2-oxoglutarate$ the effect was identified on $L-glutamate-5-semialdehyde$, for $L-glutamine$ and $4-aminobutanoate$ the effect was seen on $5-phosphoribosylamine$, for $L-glutamate$ and $4-aminobutanoate$ the effect was identified on $L-glutamine$, for $4-aminobutanoate$ and $2-oxoglutarate$ the effect was seen on $L-glutamate$. Next, considering three metabolites at a time, for $4-aminobutanoate$, $L-glutamate$ and $L-glutamine$ effect was seen on $5-phospho-D-ribose1-diphosphate$, $L-glutamate-5-semialdehyde$, $succinate$ and $L-aspartate$ whereas for $2-oxoglutarate$, $4-aminobutanoate$, $L-glutamate$ effect was seen on $D-fructose-6-phosphate$ only. Lastly, considering all the four metabolites at one time, we identified the effect on $succinatesemialdehyde$, $D-glucosamine-6-phosphate$, $succinate$, $2-oxoglutaramate$ and $D-fructose-6-$

$phosphate$ respectively. We observed that the total number of affected metabolites due to these start sites, as per fire spread model was 14, which was equivalent to the total number of affected metabolites as found in the global sensitivity plot (Figs. 7d–g) [55,57].

For $\beta-alanine$ metabolism, we observed that considering $\beta-alanine$ causes maximal effect on $malonylCoA$, $2-oxoglutarate$, $L-lysine$, $3-ureidopropionate$ and $L-arginine$, whereas for $L-aspartate$ effect was seen on $L-lysine$, $3-ureidopropionate$ and $spermidine$. Moreover, considering both $\beta-alanine$ and $L-aspartate$, group effect was seen on $L-arginine$, $3-ureidopropionate$ and $spermine$, whereas for $malonylCoA$ and $L-aspartate$, group effect was observed on $L-arginine$, $3-ureidopropionate$ and $spermine$. Similarly, for $\beta-alanine$ and $malonylCoA$, group effect was observed on $L-lysine$, $L-arginine$ and $spermine$. Finally, considering $\beta-alanine$, $malonylCoA$ and $L-aspartate$, group effect was seen on $L-arginine$, $\beta-alanyl-L-arginine$ and $propenoylCoA$ respectively. Furthermore, the fire spread model suggested an effect of over 15 metabolites due to infection spread, which was identical to what global sensitivity analysis predicts, which validated our previous finding (Section S5(SI) Figs. S22 a–f in File S1) [55,56].

For $taurine-hypotaurine$ metabolism, considering $hypotaurine$ maximal effect was observed on $3-sulfoalanine$, $taurine$, $L-cysteate$, $glutaurine$, and for $taurine$, maximal effect was seen on $3-sulfoalanine$, $3-cysteiamine$, $hypotaurine$, $glutaurine$, for $3-sulfoalanine$ effect was seen on $hypotaurine$, $taurine$, $L-cysteate$ and $glutaurine$. Moreover, considering both $hypotaurine$ and $taurine$, maximal group effect was seen on $choloylCoA$, $3-sulfoalanine$, $3-cysteamine$, $3-cysteine$ and $L-cysteate$, for $hypotaurine$ and $3-sulfoalanine$ maximal group effect was seen on $glutaurine$, $taurocholate$, $3-cysteamine$, $3-cysteine$ and $L-cysteate$, whereas for $taurine$ and $3-sulfoalanine$ maximal effect was seen on $glutaurine$, $taurocholate$, $3-cysteamine$, $3-cysteine$ and $L-cysteate$ [28]. Finally, taking all three metabolites, maximal effect was seen on $glutaurine$, $taurocholate$, $3-cysteamine$, $3-cysteine$, $L-cysteate$ and $5-L-glutamyl-peptide$. Moreover, the fire spread model suggested an effect of over 12 metabolites due to infection spread, which was similar to our results shown using global sensitivity analysis, thus validating our results (Section S5(SII) Figs. S23 a–g in File S1) [45,55]. Global sensitivity analysis results on butanoate metabolism is discussed in Section S5(SIII) Figs. S24a–g in File S1.

Analyzing the damage caused in metabolic pathways due to infection spread

When we considered an infected metabolite, high burning probability resulted in greater chance that it could infect the associated metabolic pathway. Similarly, if combating probability was high, then the metabolites were cured and the associated metabolic pathway was restored. We calculated a possible range of critical values for all metabolic pathways in $H.$ $sapiens$ (Fig. S5 in File S1). It illustrated the effect of infection spread and its subsequent curing. Critical value of a particular metabolic pathway suggested the overall infection scenario, giving insight into the number of infected metabolites that could not be cured after combat analysis is performed. Table S5 (in File S1) represents the list of infected, cured and uncured metabolites. From Fig. S5 (in File S1), it was evident that metabolic pathways under carbohydrate metabolism had critical values ranging from 1 to 7 having an average of 4.59, from 1 to 35 under amino acid metabolism with average of 6.22, from 1 to 36 under lipid
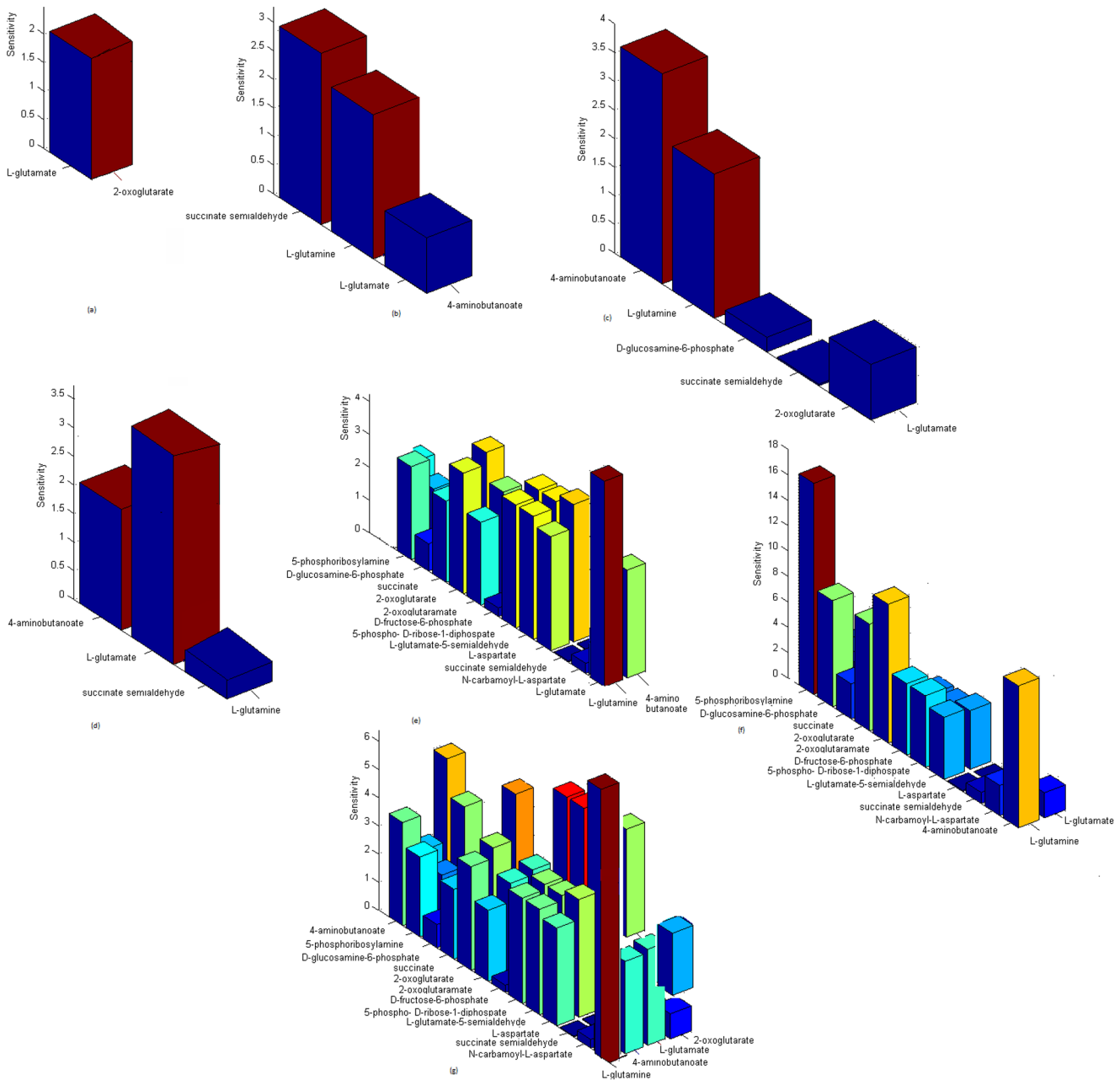
Figure 7. Plots representing global sensitivity analysis performed on glutamate metabolism for metabolites. (a) 2-oxoglutarate, (b) 4-aminobutanoate, (c) L-glutamate, (d) L-glutamine, (e) L-glutamine, 4-aminobutanoate (group effect), (f) L-glutamine, L-glutamate (group effect), and (g) L-glutamine, 4-aminobutanoate, L-glutamate, 2-oxoglutarate (group effect).
doi:10.1371/journal.pone.0069724.g007

metabolism range average of 6.89, from 1 to 4 under energy metabolism with average of 2.2 and from 1 to 8 under co-factors and vitamins metabolism with an average of 2.8 respectively (Section S6(SI–SII) Tables S5–S6 in File S1). Thus, critical value ranging from 1–5 were less prone to infection, 5–10 were more prone to infection, whereas value greater than 10 were most prone to infection [58].

This was because critical value depends on the number of metabolites cured with respect to metabolites infected [59]. A higher critical value indicated that less number of infected metabolites were cured, whereas a less critical value indicated more number of infected metabolites cured. If critical value is 0,

then all infected metabolites were cured. In case of glutamate metabolism critical value was 0, when site of infection was both L-glutamate and 4-aminobutanoate. This signifies the fact that all the metabolites that became infected due to selection of either L-glutamate or 4-aminobutanoate were cured. In case of β-alanine metabolism, critical value was 0 when start site of infection was β-alanine, whereas it was 1 when infection start site was L-aspartate, indicating that L-aspartate remained infected even after the combat process was over [60]. In case of taurine and hypotaurine metabolism critical value was observed to be 0 (infection start site = 3-sulfino-L-alanine and taurine), whereas it was 4 when infection start site was L-cysteate. For the later case, reason for

high critical value was due to the unsuccessful combat mechanismn, in which taurine, L-cysteate, taurocholate and 5-glutamyl taurine remained infected. Furthermore, in butanoate metabolism critical value was 0 when infection start site was 4-aminobutanoate, whereas it was 4 when infection start site was L-glutamate as the 4-aminobutanoate, succinate semialdehyde, succinate and L-glutamate remain infected even after combat process ends. The critical values could be further used to analyze the degree of fitness of a metabolic pathway in case of infection spread, and could be further utilized to study the robustness of the metabolites involved in a metabolic pathway. Furthermore, we have also performed various perturbations on the given metabolic pathways (as discussed in Section 'Modeling metabolic pathways quantitatively'). The various perturbation values for those metabolic pathways are shown in Tables S7–S10 (Section S7 in File S1).

Discussion

This work facilitated the study of metabolic networks and simulate the infection caused in a healthy network with implementation in certain pathways involved in Type I *Diabetes mellitus* in *H. sapiens*. The aim of this study was to evaluate whether each metabolite is infected by any chance, and the nature as well as extent of this infection. Moreover, we have also studied whether this infection spread could be combated as well as the infected metabolites could be cured. We also identified the extent of infection by calculating the critical value using both burning as well as combating probability. This simulation model considered a metabolite which was susceptible to infection via an infected metabolite. Once a metabolite was infected, it spread the infection, which harmed the network but also started recovering if there was a regulation provided to the metabolite. Also, there was a chance that this cured metabolite was again susceptible to the infection spread.

We implemented this method in four metabolic pathways for *H. sapiens* involved in Type I *Diabetes mellitus*, namely, glutamate metabolism, β-alanine metabolism, taurine and hypotaurine metabolism and butanoate metabolism. The reason for selecting these metabolic pathways was due to the involvement of two important genes GAD and INS that have major role in Type I *Diabetes mellitus*. The number of start site of infection spread for these four metabolic pathways were found to be 10, namely, L-glutamate, 4-aminobutanoate (for glutamate metabolism), β-alanine, L-aspartate (for β-alanine metabolism), 3-sulfino-L-alanine, taurine, L-cysteate, hypotaurine (for taurine and hypotaurine metabolism), and 4-aminobutanoate, L-glutamate (for butanoate metabolism). Furthermore, for tracking the path of infection spread through these infection start sites as well as identifying their containment strategy, we found the burning probability and combating probability values as 0.2 and 1 (L-glutamate), 1 and 1 (4-aminobutanoate), 0.33 and 0.5 (β-alanine), 1 and 1 (L-aspartate), 0.5 and 1 (3-sulfino-L-alanine), 0.5 and 1 (taurine), 1 and 0 (L-cysteate), 0 and 0 (hypotaurine), 1 and 1 (4-aminobutanoate), 1 and 0 (L-glutamate) respectively. Thus, out of these 10 probable start site for infection spread L-cysteate, hypotaurine and L-glutamate have no ability to combat the infection spread, whereas the other metabolites have the combating ability ranging from 33% to 100%. These ten probable infection start sites may be targeted to explore the effects of long-term infection combat and cure.

For implementing the fire spread, we used strategies, based on quantitative studies and graphs. The quantitative strategy using ODEs implements the fire spread using mathematical models and expressions. For biological validation, we used the sensitivity

analysis for identifying the nature and property of these metabolites and their role in disease spread. In our model we do not consider any metabolite to become immunized to the infection spread and consider them equally susceptible to other infected metabolites against infection spread. One of the effective approaches in this case is curing the infected metabolites and vaccinating the uneffected ones with a probability proportional to their conductivities, so that a greater proportion of metabolites of high connectivity are vaccinated than metabolites with low connectivity. Another strategy is specifically targeting the hub metabolites by vaccinating all metabolites in the pathway of connectivity higher than some threshold value. The processes of infection and curing run for a specific number of iterations, depending on the number of metabolites in the metabolic pathway. We have assigned a maximum iteration value of $n/2$, where n is the total number of metabolites in the metabolic pathway. The reason for this threshold is that after the iteration value is $n/2$, the results converge and there is no further need to continue performing further iterations. After the infection is combated and the number of iterations is complete, the critical value, signifying the number of metabolites that cannot be cured, is calculated.

From our analysis, we have also found that in *H. sapiens* metabolic pathways under carbohydrate metabolism have a range of critical values from 1 to 7, under amino acid metabolism from 1 to 35, under lipid metabolism from 1 to 36, under energy metabolism from 1 to 4 and under metabolism of co-factors and vitamins from 1 to 8. Furthermore, from this study we want to mention that critical values ranging from 1–5 is less prone to infection, 5–10 is more prone to infection, whereas value greater than 10 are most prone to infection. We would also like to make a note on some recent advances in systems biology approaches, such as flux balance analysis, which have been successful in idenitfying optimal metabolic pathways and extreme pathways. But, the volume of work that have been done in correlating sensitivities, both local and global, with FBA, as well as judging the system states of a network is less. Furthermore, less work have been performed in areas of detecting and quantifying 'feedback' using certain conventional techniques like FBA. Thus, novelty of our approach lies in that we have correlated system state identification, feedback detection, as well as sensitivities studies in diseased state pathways. This investigation can be taken one step further by analyzing the density factor as well as applying time constraints to the infection caused in the metabolic networks. Finally, we can even extend this method to analyze the patterns associated with epidemiological and endemic networks.

Supporting Information

File S1 Supporting information. Figure S1. Spread of infection in glutamate metabolism with infection start site as '3'. Figure S2. Spread of infection in glutamate metabolism with infection start site as '4'. Figure S3. Combat process in glutamate metabolism with infection start site as '3'. Figure S4. Combat process in glutamate metabolism in *H. sapiens* with infection start site as '4'. Figure S5. Plot representing distribution of critical values in all metabolic pathways in *H. sapiens*. Figure S6. β-alanine metabolism; Infection start site = β-alanine. Figure S7. β-alanine metabolism; Infection start site = L-aspartate. Figure S8. β-alanine metabolism; Combat analysis for infection start site = β-alanine. Figure S9. β-alanine metabolism; Combat analysis for infection start site = L-aspartate. Figure S10. Taurine and hypotaurine metabolism; Infection start site = 3-sulfino-L-alanine. Figure S11. Taurine and hypotaurine metabolism; Infection start site = taur-

ine. Figure S12. Taurine and hypotaurine metabolism; Combat analysis for infection start site = 3-sulfino-L-alanine. Figure S13. Taurine and hypotaurine metabolism; Combat analysis for infection start site = taurine. Figure S14. Taurine and hypotaurine metabolism; Combat analysis for infection start site = L-cysteate. Figure S15. Taurine and hypotaurine metabolism; Infection start site = L-cysteate. Figure S16. Taurine and hypotaurine metabolism; Infection start site = hypotaurine. Figure S17. Butanoate metabolism; Infection start site = 4-aminobutanoate. Figure S18. Butanoate metabolism; Infection start site = L-glutamate. Figure S19. Butanoate metabolism; Combat analysis for infection start site = 4-aminobutanoate. Figure S20. Butanoate metabolism; Combat analysis for infection start site = L-glutamate. Figure S21. Feedback analysis. Figure S22. Global sensitivity analysis of β-alanine metabolism. Figure S23. Global sensitivity analysis of taurine-hypotaurine metabolism. Figure S24. Global sensitivity analysis of butanoate metabolism. Table S1. Target function, non-constant concentration of species, variable, initial concentration in glutamate metabolism. Table S2. Target function, concentration

fluxes of reactions, variable, initial concentration in β-alanine metabolism. Table S3. Target function, concentration fluxes of reactions, variable, initial concentration in taurine and hypotaurine metabolism. Table S4. Target function, concentration fluxes of reactions, variable, initial concentration in butanoate metabolism. Table S5. Identification of infected, cured and un-cured metabolites in the four metabolic pathways. Table S6. Critical value analysis in the four metabolic pathways. Table S7. Perturbations in β-alanine metabolism. Table S8. Perturbations in taurine and hypotaurine metabolism. Table S9. Perturbations in butanoate metabolism. Table S10. Perturbations in glutamate metabolism.
(DOC)

Author Contributions

Conceived and designed the experiments: ST. Performed the experiments: ST. Analyzed the data: ST RKD. Contributed reagents/materials/analysis tools: ST. Wrote the paper: ST RKD.

References

1. Nica AC, Dermitzakis ET (2008) Using gene expression to investigate the genetic basis of complex disorders. Hum Mol Genet (Suppl. R2): R129–34.
2. Nicholson JK, Lindon JC (2008) Systems biology: Metabonomics. Nature 456: 7221.
3. Zinck R, Grimm V (2009) Unifying wildfire models from ecology and statistical physics. The American Naturalist 174: E170–E185.
4. Kenah E, Robins JM (2007) Network-based analysis of stochastic SIR epidemic models with random and proportionate mixing. J Theor Biol (Suppl. 4): 706–22.
5. Rhodes CJ, Anderson RM (1998) Forest-fire as a model for the dynamics of disease epidemics. Journal of the Franklin Institute (Suppl. 2): 199–211.
6. Anderson RM, May RM (1991) Infectious diseases of humans: dynamics and control. Oxford University Press. 766 p.
7. Bak P, Chen K, Tang C (1990) A forest-fire model and some thoughts on turbulence. Phys Lett A 147: 297–300.
8. Choisy M, Gugan JF, Rohani P (2007) Mathematical Modeling of Infectious Diseases Dynamics. Encyclopedia of Infectious Diseases: Modern Methodologies. John Wiley & Sons, Inc. pp. 379–404.
9. Chitour Y, Grognard F, Bastin G (2006) Equilibria and stability analysis of a branched metabolic network with feedback inhibition. Networks and Heterogeneous Media 1(Number 1): 219–39.
10. Tomovi R (1963) Sensitivity Analysis of Dynamic Systems. McGraw-Hill, New York. 142 p.
11. Molbak AG, Christau B, Marner B, Borch-Johnsen K, Nerup J (1994) Incidence of insulin - dependent diabetes mellitus in age groups over 30 years in Denmark Diabet Med 11: 650–55.
12. Reaven GM (1988) Role of insulin resistance in human disease. Diabetes 37: 1595–607.
13. Walker M, Turnbull DM (1997) Mitochondrial related diabetes: a clinical perspective. Diabet Med 14: 1007–09.
14. Kanehisa M, Goto S, Kawashima S, Okuno Y, Hattori M (2003) The KEGG resource for deciphering the genome. Nucleic Acids Research 32 Database issue: D277–80.
15. Funahashi A, Jouraku A, Kitano H (2004) Converting KEGG pathway database to SBML. 8th Annual International Conference on Research in Computational Molecular Biology (RECOMB 2004).
16. Hucka M, Finney A, Sauro HM, Bolouri H, Doyle JC, et al. (2003) The systems biology markup language (SBML): a medium for representation and exchange of biochemical network models. Bioinformatics (Suppl. 4): 524–31.
17. Kot M (2001) Elements of Mathematical Ecology. Cambridge University Press, Cambridge. 453 p.
18. Turchin P, Hanski I (2001) Contrasting alternative hypotheses about rodent cycles by translating them into parametrized models. Ecol Lett 4: 267–76.
19. Bailey NTJ (1975) The Mathematical Theory of Infectious Diseases and its Applications. Hafner Press, New York. 430 p.
20. Nokes DJ, Anderson RM (1988) The use of mathematical models in the epidemiology study of infectious diseases and in the design of mass vaccination programmes. Epidemiol Infect 101: 1–20.
21. Arita M (2004) The metabolic world of Escherichia coli is not small. PNAS (Suppl. 6): 1543–1547.
22. Murray JD (2002) Mathematical Biology. Springer-Verlag. 164 p.
23. Keeling MJ, Eames KT (2005) Networks and epidemic models. J R Soc Interface (Suppl. 4): 295–307.
24. Trapman P (2007) On analytical approaches to epidemics on networks. Theor Popul Biol (Suppl. 2): 160–73.
25. Lindner B, Doiron B, Longtin A (2005) Theory of oscillatory firing induced by spatially correlated noise and delayed inhibitory feedback. Phys Rev E 72: 061919.
26. Nestorov IA (1999) Sensitivity analysis of pharmacokinetic and pharmacodynamic systems: I. a structural approach to sensitivity analysis of physiologically based pharmacokinetic models. Journal of Pharmacokinetics and Biopharmaceutics (Suppl. 6): 577.
27. Rabitz H, Kramer M, Dacol D (1983) Sensitivity analysis in chemical kinetics. Annual Review of Physical Chemistry (Suppl. 419): 161.
28. Sobol IM (1993) Sensitivity estimates for nonliner mathematical models. Mathematical modeling and computational experiments (Suppl. 4): 577–596.
29. Newman ME (2002) Spread of epidemic disease on networks. Phys Rev E Stat Nonlin Soft Matter Phys 66(Suppl. 1 Pt 2): 016128.
30. Akkanen MJ, Kivela S, Koistinen V, Sintonen H, Tuomilehto J (2009) Inpatient care of patients with type 1 diabetes mellitus by duration of diabetes and sex: A nationwide population-based longitudinal study. Risk Management and Healthcare Policy (Suppl. 2): 55–64.
31. Apgar JF, Toettcher JE, Endy D, White FM, Tidor B (2008) Stimulus design for model selection and validation in cell signaling. PLoS Comput Biol (Suppl. 2: e30.
32. Alvarez-Vasquez F, Riezman H, Hannun YA, Voit EO (2011) Mathematical Modeling and Validation of the Ergosterol Pathway in Saccharomyces cerevisiae. PLoS ONE (Suppl. 12): e28344.
33. Graciano MF, Valle MM, Kowluru A, Curi R, Carpinelli AR (2011) Regulation of insulin secretion and reactive oxygen species production by free fatty acids in pancreatic islets. Islets (Suppl. 5): 213–23.
34. Samokhvalov V, Ussher JR, Fillmore N, Armstrong IK, Keung W, et al. (2012) Inhibition of malonyl-CoA decarboxylase reduces the inflammatory response associated with insulin resistance. Am J Physiol Endocrinol Metab (Suppl. 12): E1459–68.
35. Chambers KT, Leone TC, Sambandam N, Kovacs A, Wagg CS, et al. (2011) Chronic inhibition of pyruvate dehydrogenase in heart triggers an adaptive metabolic response. J Biol Chem (Suppl. 13): 11155–62.
36. Saggerson D (2008) Malonyl-CoA, a key signaling molecule in mammalian cells. Annu Rev Nutr 28: 253–72.
37. Coburn SP (1996) Modeling vitamin B6 metabolism. Adv Food Nutr Res (Suppl. 5): 107–32.
38. Abbasi A, Corpeleijn E, van der Schouw YT, Stolk RP, Spijkerman A, et al. (2012) Parental history of type 2 diabetes and cardiometabolic biomarkers in offspring. Eur J Clin Invest (Suppl. 9): 974–82.
39. Everaert I, Taes Y, De Heer E, Baelde H, Zutinic A, et al. (2012) Low plasma carnosinase activity promotes carnosinemia after carnosine ingestion in humans. Am J Physiol Renal Physiol (Suppl. 12): F1537–44.
40. Lorenzo MP, Navarrete A, Balderas C, Garcia A (2013) Optimization and validation of a CE-LIF method for amino acid determination in biological samples. J Pharm Biomed Anal 73: 116–24.
41. Tsiani E, Abdullah N, Fantus IG (1997) Insulin-mimetic agents vanadate and pervanadate stimulate glucose but inhibit amino acid uptake. Am J Physiol 272(Suppl. 1 Pt 1): C156–62.
42. Baldzizhar R, Fedorchuk C, Jha M, Rathinam C, Henegariu O, et al. (2013) Anti-serpin antibodymediated regulation of proteases in autoimmune diabetes. J Biol Chem (Suppl. 3): 1612–9.
43. Tappia PS, Xu YJ, Rodriguez-Leyva D, Aroutiounova N, Dhalla NS (2013) Cardioprotective effects of cysteine alone or in combination with taurine in diabetes. Physiol Res (Suppl. 2): 171–8.

44. Al-Mutairi HF, Mohsen AM, Al-Mazidi ZM (2007) Genetics of Type 1 Diabetes Mellitus. Kuwait Medical Journal (Suppl. 2): 107–115.

45. Jain SK (2012) L-cysteine supplementation as an adjuvant therapy for type-2 diabetes. Can J Physiol Pharmacol (Suppl. 8): 1061–4.

46. Imae M, Inoue Y, Fu Z, Kato H, Noguchi T (2000) Gene expression of the three members of hepatocyte nuclear factor-3 is differentially regulated by nutritional and hormonal factors. J Endocrinol (Suppl. 1): R1–5.

47. Ripps H, Shen W (2012) Review: taurine: a 'very essential' amino acid. Mol Vis 18: 2673–86.

48. Cammisotto PG, Glinas Y, Deshaies Y, Bukowiecki LJ (2005) Regulation of leptin secretion from white adipocytes by insulin, glycolytic substrates, and amino acids. Am J Physiol Endocrinol Metab (Suppl. 1): E166–71.

49. Ludvigsson J (2012) Novel therapies in the management of type I diabetes mellitus. Panminerva Med (Suppl. 4): 257–70.

50. Verrotti A, Scaparrotta A, Olivieri C, Chiarelli F (2012) Seizures and type 1 diabetes mellitus: current state of knowledge. Eur J Endocrinol (Suppl. 6): 749–58.

51. Burton FR, Burton MS, Garvin PJ, Joshi SN (1992) Enteral pancreatic enzyme feedback inhibition of the exocrine secretion of the human transplanted pancreas. Transplantation (Suppl. 6): 988–92.

52. Skyler JS (2013) Primary and secondary prevention of Type 1 diabetes. Diabet Med (Suppl. 2): 161–9.

53. Bell JA, Volpi E, Fujita S, Cadenas JG, Rasmussen BB (2006) Dysregulation of muscle fatty acid metabolism in type 2 diabetes is independent of malonyl-CoA. Diabetologia (Suppl. 9): 2144–52.

54. Koshiyama H, Hamamoto Y, Honjo S, Wada Y, Lkeda H (2006) Hypothalamic pathogenesis of type 2 diabetes. Med Hypotheses (Suppl. 2): 307–10.

55. Gylvin T, Nolse R, Hansen T, Nielsen EM, Bergholdt R, et al. (2004) Mutation analysis of suppressor of cytokine signalling 3, a candidate gene in Type 1 diabetes and insulin sensitivity. Diabetologia (Suppl. 7): 1273–7.

56. Kawasaki T, Hashimoto K, Goto S, Kawano S, Aoki-Kinoshita KF, et al. (2006) KEGG as a glycome informatics resource. Glycobiology 16: 63R–70R.

57. Ray S, Sarkar D, Ganguly S, Maiti A (2012) An unusual presentation of latent autoimmune diabetes in adults. Med J Malaysia (Suppl. 1): 116–7.

58. Wang JH, Byun J, Pennathur S (2010) Analytical approaches to metabolomics and applications to systems biology. Semin Nephrol (Suppl. 5): 500–11.

59. Tran LM, Rizk ML, Liao JC (2008) Ensemble modeling of metabolic networks. Biophys J (Suppl. 12): 5606–17.

60. Casals M, Guzman K, Cayla JA (2009) Mathematical models used in the study of infectious diseases. Rev Esp Salud Publica (Suppl. 5): 689–95.